Carbonate-silicate melt immiscibility, REE mineralising fluids, and the evolution of the Lofdal Intrusive Suite, Namibia

Sarah Bodeving[a,*], Anthony E. Williams-Jones[a], and Scott Swinden[b]

[a] Department of Earth and Planetary Sciences, McGill University, 3450 University Street, Montreal, QC, Canada H3A 0E8; anthony.williams-jones@mcgill.ca

[b] Swinden Geoscience Consultants, 224 Main Street, Wolfville, NS, Canada B4P 1C4; geoswin@gmail.com

* corresponding author email address sarah.bodeving@mail.mcgill.ca, telephone number +1 514 222 5273 (S. Bodeving).

Bodeving, S., Williams-Jones, A.E., Swinden, S., 2017. Carbonate–silicate melt immiscibility, REE mineralising fluids, and the evolution of the Lofdal Intrusive Suite, Namibia. Lithos 268–271, 383-398. http://dx.doi.org/10.1016/j.lithos.2016.11.024.

ABSTRACT

The Lofdal Intrusive Suite, Namibia, consists of calcio-carbonatite and silica-undersatured alkaline intrusive rocks ranging in composition from phono-tephrite to phonolite (and nepheline syenite). The most primitive of these rocks is the phono-tephrite, which, on the basis of its Y/Ho and Nb/Ta ratios, is interpreted to have formed by partial melting of the mantle. Roughly linear trends in major and trace element contents from phono-tephrite to phonolite and nepheline syenite indicate that the latter two rock types evolved from the phono-tephrite by fractional crystallisation. The nepheline syenite, however, has a lower rare earth element (REE) content than the phonolite. The carbonatite has a primitive mantle-normalised REE profile roughly parallel to that of the silica-undersaturated alkaline rocks, although the absolute REE concentrations are higher. Like the phono-tephrite, it also has a mantle Y/Ho ratio. However, the Nb/Ta and Zr/Hf ratios are significantly higher. Moreover, the carbonatite displays strong negative Ta, Zr and Hf anomalies on spidergrams, whereas the silicate rocks display positive anomalies for these elements. Significantly, this behaviour is predicted by the corresponding carbonatite-silicate melt partition coefficients, as is the behaviour of the REE. Based on these observations, we interpret the carbonatite to represent an immiscible liquid that exsolved from the phono-tephrite or possibly the phonolite melt. The result was a calcio-carbonatite that is enriched in the heavy REE (HREE) relative to most other carbonatites. Fluids released from the corresponding magma are interpreted to have been the source of the REE mineralisation that is currently the target of exploration.

Bodeving, S., Williams-Jones, A.E., Swinden, S., 2017. Carbonate–silicate melt immiscibility, REE mineralising fluids, and the evolution of the Lofdal Intrusive Suite, Namibia. Lithos 268–271, 383-398. http://dx.doi.org/10.1016/j.lithos.2016.11.024.

KEYWORDS: Alkaline; Carbonatite; Fenitisation; Liquid Immiscibility; Rare Earth Elements; Silica-Undersaturated.

1. INTRODUCTION

Three petrogenetic models have been proposed for the generation of carbonatitic magmas. Seeking to explain the close spatial association of carbonatites with silica-undersaturated alkaline rocks, two of these models invoke a parental silicate melt. One of them involves the separation of an immiscible carbonatite magma from a silicate magma (von Eckermann, 1948; Kjarsgaard and Hamilton, 1988; Kjarsgaard and Hamilton, 1989; Gittins, 1989; Le Bas, 1989; Kjarsgaard et al., 1995; Veksler et al., 1998b, 2012; Martin et al., 2013; Weidendorfer et al., 2016) and the other the formation of a residual carbonatitic magma from a CO_2-enriched silicate melt by fractional crystallisation (King, 1949; Watkinson and Wyllie, 1971; Lee and Wyllie, 1994; Lee and Wyllie, 1998a). A combination of the two has also been proposed, in which extreme fractionation of the silicate magma drives the melt composition into the carbonate-silicate immiscibility field (Weidendorfer et al., 2016). The third model postulates direct partial melting of a carbonated mantle peridotite (Wyllie and Tuttle, 1960; Wallace and Green, 1988; Sweeney, 1994; Dalton and Presnall, 1998; Wyllie and Lee, 1998; Gudfinnsson and Dalton, 2005; Mitchell, 2005; Dasgupta and Hirschmann, 2007; Dasgupta et al., 2009; Ghosh et al., 2009). There is, however, no consensus on which of these models best explains the genesis of carbonatites, possibly because a single model cannot satisfactorily account for the wide range of compositions and associations displayed by carbonatites globally.

In this paper, we report results of a study of the Lofdal Intrusive Suite, Namibia, in which calcio-carbonatites (as dykes) are spatially associated with phono-tephrite and

Bodeving, S., Williams-Jones, A.E., Swinden, S., 2017. Carbonate–silicate melt immiscibility, REE mineralising fluids, and the evolution of the Lofdal Intrusive Suite, Namibia. Lithos 268–271, 383-398. http://dx.doi.org/10.1016/j.lithos.2016.11.024.

phonolite dykes, form a separate pluton (Emanya) and intrude a nepheline syenite pluton (Main Intrusion). Major/trace element and stable isotope data are used to reconstruct the evolution of the intrusive suite, evaluate the three petrogenetic models that have been proposed for the formation of carbonatites and make inferences about the source of the fluids responsible for the REE mineralisation currently being explored in the area.

2. REGIONAL GEOLOGY

The Lofdal carbonatites and associated nepheline syenites are located in Damaraland, northwest Namibia (Fig. 1). They comprise a main intrusion and several satellite intrusions that are accompanied by a large number of silicate dykes, varying in composition from phono-tephrite to phonolite. Carbonatite dykes are also observed. The intrusions were emplaced in the Huab Metamorphic Complex (HMC) in the Paleoproterozoic Welwitschia inlier, which, together with the Kamenjab and Braklaagte inliers, forms the exposed southern edge of the Archean Congo Craton (Miller, 2008). Rocks forming the HMC are estimated by Frets (1969) to have an age of >1700 Ma and comprise gneisses, schists, amphibolites, quartzites and arkoses. The Damara mobile belt, which separates the Congo Craton from the Kalahari Craton, belongs to the Pan African system of mobile belts that formed during the fusion of the Gondwana supercontinent (Gray et al., 2008). The volcanic and sedimentary rocks of this belt, e.g., the Nosib Group, including the Naauwpoort Formation, owe their origins to rifting between ~1000 Ma and 750 Ma (Porada, 1989; Gray et al., 2008); the alkali rhyolites of the Naauwpoort Formation have been dated at 752 ± 7 Ma (U-Pb zircon; de Kock et al., 2000). This rifting produced a large sedimentary basin with several prongs that were subsequently deformed by compressional forces into the intracontinental Damara belt and the coastal Gariep and Kaoko belts (Gray et al., 2008). The Lofdal Intrusive Suite, within the

Bodeving, S., Williams-Jones, A.E., Swinden, S., 2017. Carbonate–silicate melt immiscibility, REE mineralising fluids, and the evolution of the Lofdal Intrusive Suite, Namibia. Lithos 268–271, 383-398. http://dx.doi.org/10.1016/j.lithos.2016.11.024.

analytical uncertainty, is the same age (754 ± 8Ma, U-Pb titanite; Jung et al., 2007) as the alkali rhyolites of the Naauwpoort Formation and the quartz normative Oas syenite, which is located immediately southwest of the Lofdal Intrusive Suite (756 ± 2 Ma, U-Pb zircon; Hoffman et al., 1996). We therefore conclude that they are all coeval and were emplaced during the continental rifting event that produced the Damara basin. In the west, sub-horizontal Karoo sediments (~180 Ma; Duncan et al., 1997) and lavas overlie the basement rocks of the HMC and parts of the Oas syenite (Frets, 1969).

3. METHODOLOGY

Fieldwork was guided by detailed geological maps prepared for Namibia Rare Earths Inc., a Canadian junior exploration company, evaluating rare earth element mineralisation spatially associated with the Lofdal Intrusive Suite. This involved establishing the field relationships of the different lithological units and sampling outcrops for subsequent petrographic study. Drill core made available by Namibia Rare Earths Inc. was also sampled. Petrographic observations were made using an optical microscope in transmitted and reflected light and a scanning electron microscope (SEM).

The mineral chemistry was determined at McGill University using a JEOL JXA-8900L electron microprobe equipped with five WDS spectrometers and a Si(Li) EDS detector. A ZAF correction procedure was used for reduction of the data. The thin sections were carbon-coated prior to analyses. Mica, feldspar and cancrinite were analysed at 15 kV, with a beam diameter of 5 μm and a beam current of 20 nA. Analyses of pyroxene and nepheline were conducted at 15 kV, with a beam diameter of 10 μm and a current of 20 nA. Calcite was analysed with an acceleration voltage of 15 kV, a beam diameter of 15 μm and a current of 20 nA, zircon at 20 kV, with a beam diameter of 5 μm and a current of 30 nA, and

Bodeving, S., Williams-Jones, A.E., Swinden, S., 2017. Carbonate–silicate melt immiscibility, REE mineralising fluids, and the evolution of the Lofdal Intrusive Suite, Namibia. Lithos 268–271, 383-398. http://dx.doi.org/10.1016/j.lithos.2016.11.024.

apatite at 20 kV, a beam diameter of 10 μ m beam and a current of 30 nA. The results of the analyses are reported in supplementary material (ESM_1).

Samples from outcrop and core from one drill hole were analysed for their bulk rock composition at Activation Laboratories Ltd. (ActLabs) in Ancaster, Ontario. The samples were crushed, riffled and pulverised in a steel mill to >95 % -200 mesh. They were analysed with a code 8-REE Assay Package (REE-Na-Zr-Y-Ta-U-Th-Be-P-Sn ICP-OES and ICP-MS Assay package) involving the application of a multi-acid digestion and lithium metaborate/tetraborate fusion with subsequent detection of major and trace elements by ICP-OES and ICP-MS, respectively. The Loss of Ignition (LOI) was determined after fusion. The accuracy was tested using standards (Amis 185 and in-house standards, Std 4, Std 5, developed by Namibia Rare Earths Inc.), which were inserted after each batch of approximately 20 samples. Potential contamination during analysis was tested by the addition of blanks (marble), and the precision of the analyses tested through the inclusion of duplicates. In addition, Activation Laboratories Ltd. conducted an internal quality control. The full data set, containing the analyses of duplicates, blanks and standards, is available in the supplementary material (ESM_1) and averages of the different rock types are presented in Table 1.

Carbon and oxygen isotopic analyses of carbonatite were carried out at the McGill Stable Isotope Laboratory. Samples were collected for analysis in the form of dry powder using a micro-drill. Approximately 120 µg of sample powder was introduced into glass vials and loaded into a Nu Carb Carbonate Device™ interfaced with a Dual Inlet Isotope Ratio System and a Nu Instruments Perspective™ mass spectrometer. The device automates the sample preparation and the measurements. The powder was reacted with orthophosphoric acid at a temperature of 70 °C and cryogenically transferred through a dual micro-inlet to the mass spectrometer for analysis. The data are reported in standard δ-notation, relative to V-

Bodeving, S., Williams-Jones, A.E., Swinden, S., 2017. Carbonate–silicate melt immiscibility, REE mineralising fluids, and the evolution of the Lofdal Intrusive Suite, Namibia. Lithos 268–271, 383-398. http://dx.doi.org/10.1016/j.lithos.2016.11.024.

SMOW for $\delta^{18}O$ and V-PDB for $\delta^{13}C$. Regular analyses of in-house standards demonstrated that the precision for both $\delta^{18}O$ and $\delta^{13}C$ was better than ±0.03‰. The resulting isotope data are listed in Table 2.

4. LOFDAL INTRUSIVE SUITE

4.1. Field relationships

The geology of the Lofdal Intrusive Suite was first described by Frets (1969), who recognised a large intrusion of quartz syenite in the southwest (Oas syenite), nepheline normative syenite in the centre and E-W striking tinguaite dykes, although he did not note the occurrence of carbonatite. The largest member of this suite is the NE-SW trending Main Intrusion that occupies an area of ~2 km^2 (Fig. 1), and is composed of nepheline syenite (locally small vertical variations in grain size and colour are suggestive of crystal settling) and later plugs and dykes of carbonatite (Fig. 2a). Contacts between the carbonatite and nepheline syenite are marked by a halo of fenitised nepheline syenite (Fig. 2b), which we interpret to have formed by interaction of the nepheline syenite with carbo-hydrothermal fluids exsolved from the carbonatitic magma. Locally, the fenites are strongly brecciated and form a carapace on top of the carbonatite plugs. There are two smaller satellite nepheline syenite plugs and a 350 m wide carbonatite plug (the Emanya intrusion) to the southwest of the Main Intrusion (Fig. 1). Diatreme (carbonate matrix) (Fig. 2c) and igneous (phonolite matrix) breccias cut the northeast and southern rim of the Main Intrusion and the margins of the two satellite nepheline syenite intrusions.

Hundreds of NE-SW trending dykes (previously referred to as the Bergville Dyke swarm; Miller, 2008) form a roughly 2-3 km wide corridor that extends for more than 5 km northeast and southwest of the Main Intrusion and follows the regional foliation. Many cross-

Bodeving, S., Williams-Jones, A.E., Swinden, S., 2017. Carbonate–silicate melt immiscibility, REE mineralising fluids, and the evolution of the Lofdal Intrusive Suite, Namibia. Lithos 268–271, 383-398. http://dx.doi.org/10.1016/j.lithos.2016.11.024.

149 cut the Main Intrusion, nepheline syenite satellite plugs and the basement, but chilled margins
150 are rarely observed and, if so, are only a few mm thick. Most of the dykes are phonolites,
151 although smaller numbers of phono-tephrite and carbonatite dykes are observed; phono-
152 tephrite dykes were not observed in the Main Intrusion and satellite plugs. The phono-
153 tephrite dykes are closely associated with the phonolite dykes, although temporal
154 relationships between them could not be determined. Locally, both types of dykes have been
155 folded (Fig. 2d). The carbonatite dykes, which vary in width from <10cm to 10's of metres,
156 are concentrated within a few hundred metres of the Main Intrusion. A very prominent
157 feature of the landscape is the occurrence of narrow 2-3 m wide NE-SW trending ridges,
158 locally up to 1 m high that, in some cases, cut phonolite dykes. These were formerly
159 interpreted to be carbonatite dykes (Wall et al., 2008; do Cabo, 2014), but have been shown
160 to comprise albitite that was brecciated and replaced by carbonate minerals (Wollenberg et
161 al., in prep). They are currently being explored by Namibia Rare Earths Inc. as a possible
162 source of REE.
163

164 **4.2 Nepheline syenite**

165 The nepheline syenite is grey, holocrystalline, phaneritic and locally pegmatitic; the grain-
166 size varies between 2mm and <10cm. The major rock-forming minerals were K-feldspar and
167 nepheline. Fresh nepheline is very rare but its former occurrence is indicated by
168 pseudomorphs with square cross-sections, in which the nepheline was replaced by cancrinite
169 or sodalite; a very small proportion of pseudomorphs contain relict nepheline (supplementary
170 material ESM_2_1a). Most of the K-feldspar is in the form of variably sericitised microcline,
171 although perthite is locally observed. The main mafic mineral, clinopyroxene, is present
172 dominantly as subhedral phenocrysts that vary in composition from aegirine to aegirine-
173 augite. Locally, partial to complete rim to core replacement by biotite is evident; biotite also

Bodeving, S., Williams-Jones, A.E., Swinden, S., 2017. Carbonate–silicate melt immiscibility, REE mineralising fluids, and the evolution of the Lofdal Intrusive Suite, Namibia. Lithos 268–271, 383-398. http://dx.doi.org/10.1016/j.lithos.2016.11.024.

occurs as a primary mineral. Zircon, titanite, apatite and pyrochlore are accessory phases (supplementary material ESM_2_1b).

A feature of the Main Intrusion is that the proportion of nepheline increases from the margins of the intrusion inwards and its habit changes from interstitial to phenocrystic in the same direction. At the margins, tabular K-feldspar is the main rock-forming mineral and the mafic minerals, clinopyroxene and biotite are present in lesser proportions than elsewhere in the intrusion.

4.3. Carbonatite

Carbonatite occurs mainly in the Main Intrusion (and at Emanya, Fig. 1). There, it intrudes nepheline syenite, and is associated with brecciation and fenitisation of the latter. Magmatic flow-banding is common as are stoped fenitised nepheline syenite blocks. The carbonatite takes the form of coarse-grained plugs and dykes that vary in colour from grey (mainly) to brown on weathered surfaces; their interiors are white. Based on their modal mineralogy (> 90 vol.% anhedral to subhedral calcite) they are calcio-carbonatites (Gittins and Harmer, 1997). Clinopyroxene is the only other mineral in appreciable proportions (up to 10 vol.%) and occurs in association with lesser proportions of hexagonally-shaped apatite and oscillatory-zoned idiomorphic pyrochlore (supplementary material ESM_2_1c). These minerals form magmatic segregations that help define the flow-banding. The minor minerals are K-feldspar, biotite, magnetite, titanite and the LREE-minerals monazite-(Ce) and parasite-(Ce), which are usually observed intergrown with or as inclusions in aegirine, apatite and pyrochlore phenocrysts.

Bodeving, S., Williams-Jones, A.E., Swinden, S., 2017. Carbonate–silicate melt immiscibility, REE mineralising fluids, and the evolution of the Lofdal Intrusive Suite, Namibia. Lithos 268–271, 383-398.
http://dx.doi.org/10.1016/j.lithos.2016.11.024.

198 **4.4. Silicate Dykes**

199 *4.4.1. Phono-tephrite dykes*

200 Phono-tephrite dykes are found only northeast of the Main Intrusion in close
201 proximity to phonolite dykes. These dykes are dark grey to black in colour and vary from
202 several cm to half a metre in width. They are locally deformed and show evidence of strong
203 carbonate alteration. Phenocrysts < 1cm in diameter with dark rims and lighter cores are
204 visible macroscopically. They comprise pseudomorphs filled with a very fine-grained
205 mixture of calcite and biotite; their margins are defined by fine-grained biotite. Locally augite
206 phenocrysts, containing zircon and titanite inclusions, were largely replaced by epidote.
207 Generally, the groundmass consists of biotite, albite, lesser calcite and accessory ilmenite,
208 barite and quartz. In addition, amygdules filled with calcite are common (Fig. 2d).

209 *4.4.1. Phonolite dykes*

210 The silicate dykes of the Lofdal Intrusive Suite are dominantly phonolites that vary
211 from trachytic to porphyritic. The phenocrysts range up to 0.5 cm in diameter and consist
212 mainly of microcline (the primary magmatic phase was likely sanidine) (supplementary
213 material ESM_2_1d). Pseudomorphs of cancrinite after nepheline, subhedral apatite,
214 glomerophyritic biotite and idiomorphic magnetite make up the other phenocryst phases. The
215 matrix consists mostly of fine-grained biotite, albite and K-feldspar and lesser calcite.
216 Magnetite, apatite and zircon occur as accessory minerals in the groundmass. A flow texture
217 is commonly evident from the alignment of the groundmass minerals around the larger
218 phenocrysts. Evidence of deformation in the form of aligned and stretched phenocrysts was
219 observed in several dykes. As in the phono-tephrite, amygdules filled with calcite are
220 common.

221

Bodeving, S., Williams-Jones, A.E., Swinden, S., 2017. Carbonate–silicate melt immiscibility, REE mineralising fluids, and the evolution of the Lofdal Intrusive Suite, Namibia. Lithos 268–271, 383-398.
http://dx.doi.org/10.1016/j.lithos.2016.11.024.

4.5 Breccia

Breccias are prominently exposed on the northeast and southern rim of the Main Intrusion, and on the margins of the two satellite nepheline syenite plugs. They are clast-supported and are characterised by poorly-sorted angular to rounded fragments, ranging from <1cm to several m in diameter (Fig. 2c). The fragments comprise deformed basement rocks of the Huab Metamorphic Complex, e.g., gneiss and amphibolite, and also nepheline syenite (within the intrusions). Some of the basement fragments are flooded with aegirine-augite, which envelops individual albite grains in the gneiss. In addition, calcite appears as inclusions in the albite. The breccia matrix is either composed of phonolite, (comprising albite and calcite, and lesser biotite and aegirine-augite, with the latter two minerals also occurring as glomerophyritic phenocrysts) or consists exclusively of calcite. We interpret the former to identify the breccia as intrusive and the latter as a diatreme.

4.6 Fenite

The nepheline syenite in contact with carbonatite in the Main Intrusion underwent intense fenitisation, which destroyed the original texture and mineralogy. Depending on the nature of the adjacent intrusion, i.e., carbonatite plug or dyke, the fenitised zone varies in thickness from 50 cm up to several metres (Fig. 2b). The fenite consists dominantly of anhedral to subhedral K-feldspar (microcline) and lesser albite and calcite. Rare aegirine-augite, partially replaced by calcite, and abundant apatite and zircon and less common pyrochlore, titanite and magnetite are preserved as accessory minerals from the nepheline syenite in the fenites. Zirconolite and columbite-(Fe) occur in very minor amounts.

Bodeving, S., Williams-Jones, A.E., Swinden, S., 2017. Carbonate–silicate melt immiscibility, REE mineralising fluids, and the evolution of the Lofdal Intrusive Suite, Namibia. Lithos 268–271, 383-398.
http://dx.doi.org/10.1016/j.lithos.2016.11.024.

5. MINERAL CHEMISTRY

5.1. Carbonate

The carbonate mineral in the calcio-carbonatite, fenite, nepheline syenite and the diatreme breccia is calcite, which, within the analytical uncertainty, has the same composition in each of these lithological units. It contains minor concentrations of Mg, Fe, Mn and Sr (supplementary material ESM_1)

5.2. Feldspar

Coarse-grained or phenocrystic potassium feldspar (microcline) present in nepheline syenite, phonolite, carbonatite and fenite, has a composition of Or_{91-97}, whereas the feldspar in the matrix of the nepheline syenite, the carbonatite and the fenite is albite with a composition close to that of its end member, i.e., Ab_{94-99} (supplementary material ESM_1 and ESM_2_2).

5.3. Feldspathoid minerals

Nepheline fresh enough for reliable electron microprobe analyses could only be found in two samples, both in nepheline syenite from the Main Intrusion (NLOFDR3353, NLOFDR3356). It has a composition close to that corresponding to the empirical formula of $Na_{0.75}K0_{,25}AlSiO_4$ and contains very minor concentrations of Fe and Ca (supplementary material ESM_1).

The composition of cancrinite (supplementary material ESM_1) shows little variation in either nepheline syenite or phonolite. Based on the relative proportions of the non-volatile components, it is close to the end-member cancrinite composition, differing from the latter mainly by the presence of a small proportion of Sr. The low totals of ~ 91 wt.% reflect unknown proportions of molecular water, carbonate and possible hydroxyl ions.

5.4. Ferromagnesian minerals

Bodeving, S., Williams-Jones, A.E., Swinden, S., 2017. Carbonate–silicate melt immiscibility, REE mineralising fluids, and the evolution of the Lofdal Intrusive Suite, Namibia. Lithos 268–271, 383-398. http://dx.doi.org/10.1016/j.lithos.2016.11.024.

5.4.1. Biotite

Biotite was analysed in nepheline syenite, phonolite, phono-tephrite, carbonatite and the intrusive breccia, and may be subdivided into three compositional groups, namely a Fe-rich group (annite), a Fe-poor group (phlogopite) and a group of intermediate composition (supplementary material ESM_1 and ESM_2_3). The annite group comprises phenocrysts and secondary vein-hosted biotite in the nepheline syenite, and phenocryst- and groundmass-biotite in the phonolite. However, the phonolite-hosted biotite is generally richer in Fe than that in the nepheline syenite. Phlogopite is only present in the groundmass of the strongly altered phono-tephrite and the breccia matrix and the compositionally intermediate biotite is restricted to carbonatite.

5.4.2. Clinopyroxene

Based on its composition, the clinopyroxene of the calcio-carbonatite is aegirine, whereas that in the nepheline syenite varies from aegirine to aegirine-augite (supplementary material ESM_2_4).

5.5. HFSE and REE-bearing minerals

The main primary high-field-strength-elements (HFSE) and REE-bearing minerals in the Lofdal Intrusive Suite are pyrochlore, apatite and zircon. Zircon and apatite occur commonly in all of the major rock types of the suite, whereas pyrochlore is mainly restricted to the calcio-carbonatite, however, it also has been identified in nepheline syenite. These three minerals largely account for the elevated concentrations of the REE, Th, Nb, Hf and Zr in the carbonatites and alkaline silicate rocks of the suite.

5.5.1. Zircon

Zircon was analysed in carbonatite, nepheline syenite and fenite, and was found to contain minor concentrations of Hf and trace concentrations of Y and Nb, irregularly

Bodeving, S., Williams-Jones, A.E., Swinden, S., 2017. Carbonate–silicate melt immiscibility, REE mineralising fluids, and the evolution of the Lofdal Intrusive Suite, Namibia. Lithos 268–271, 383-398.
http://dx.doi.org/10.1016/j.lithos.2016.11.024.

293 distributed through the crystals; other potential trace elements were not detected
294 (supplementary material ESM_1).

295 *5.5.2. Pyrochlore*

296 Pyrochlore compositions were analysed by Gaudet (2013) in carbonatite, nepheline
297 syenite and fenite (supplementary material ESM_1). Based on its composition, most of the
298 pyrochlore classifies as oxycalciopyrochlore. In addition to its essential components, this
299 pyrochlore also contains an average of 2.3 to 2.9 wt.% total REE oxides, 1.2 to 2.2 % Ta_2O_5,
300 and 0.3 to 1.2 wt. % UO_2. A uranium-rich variety, uranpyrochlore, containing 15.5 wt% UO_2,
301 is observed locally as a replacement of carbonatite-hosted oxycalciopyrochlore crystals and
302 as oscillatory zones within the latter.

303 *5.5.3. Apatite*

304 In the calcio-carbonatite, apatite is characterised by a high content of F (3.7 wt.%) and
305 analytical totals ranging from 99 to 100 wt.%, indicating the presence of negligible OH
306 (supplementary material ESM_1). This classifies the mineral as fluorapatite; the Cl content is
307 below the limit of detection (126 ppm). In addition to its main components, the fluorapatite
308 also contains significant Sr, and minor proportions of REE, mainly the light REE.

309 The composition of apatite in the nepheline syenite is very similar to that in the
310 calcio-carbonatite (supplementary material ESM_1) and also classifies the mineral as
311 fluorapatite; F contents are locally higher in the cores of crystals. However, the concentration
312 of SiO_2 is significantly higher (0.08 vs. 0.43 wt.%) and, on average, the REE content is
313 slightly higher (0.87 vs 1.08 wt.% total REE oxides on average) than in the calcio-
314 carbonatite.

315

316

Bodeving, S., Williams-Jones, A.E., Swinden, S., 2017. Carbonate–silicate melt immiscibility, REE mineralising fluids, and the evolution of the Lofdal Intrusive Suite, Namibia. Lithos 268–271, 383-398.
http://dx.doi.org/10.1016/j.lithos.2016.11.024.

6. BULK ROCK GEOCHEMISTRY

6.1. Carbonatite

Based on their bulk rock compositions, the carbonatites all classify as calcio-carbonatite (CaO/(CaO+MnO+FeO+MgO) = 0.91); compositionally they lie close to or on the CaO-FeO boundary (supplementary material ESM_2_5). Their FeO content ranges from 0.78 to 10.06 wt.% and their MgO content averages 0.19 wt.%. The wide ranges in FeO, Na_2O, SiO_2 and P_2O_5 contents, as well as the trace elements, Ba, Sr, Zr, Hf, Nb, Th, U (supplementary material ESM_1) are due to the variable concentration of aegirine, apatite and HFSE minerals resulting from magmatic flow segregation. The primitive mantle-normalised REE profiles (Fig. 3a) are characterised by strong light REE enrichment, the absence of an Eu anomaly and a relatively flat heavy REE (from Gd to Lu) distribution. The Y/Ho ratio ranges between 25 and 32.9 and averages of 27.3, which is effectively the same as the primitive mantle ratio of 27.7 (supplementary material ESM_2_6a) (Sun and McDonough, 1989). The ratios of the geochemical twins, Nb/Ta and Zr/Hf, however, are much higher than those of primitive mantle 352.3 and 63.6 versus 17.4 and 36.2, respectively (supplementary material ESM_2_6b,c) (Sun and McDonough, 1989). Relative to the silicate rocks, the carbonatites are depleted in Ta, Pb, Zr and Hf (negative anomalies in Fig. 3b), and enriched in Sr (positive anomaly in Fig. 3b) and the light REE (LREE).

6.2. Silicate Rocks

From their mineralogy and geochemistry, the medium- to coarse-grained silicate rocks of the Main Intrusion and satellite plugs are nepheline syenites (supplementary material ESM_ 2_5). The average peralkalinity index (PI) $\{(Na_2O+K_2O)/Al_2O_3\}$ is 0.97, with the Na_2O content being slightly greater than that of K_2O (7.32 wt.% versus 6.48 wt.%) (Table 1).

Bodeving, S., Williams-Jones, A.E., Swinden, S., 2017. Carbonate–silicate melt immiscibility, REE mineralising fluids, and the evolution of the Lofdal Intrusive Suite, Namibia. Lithos 268–271, 383-398. http://dx.doi.org/10.1016/j.lithos.2016.11.024.

341 The CaO content is elevated due largely to the nearly ubiquitous alteration of nepheline to
342 cancrinite, which was also responsible for an increase in Sr and Ba concentration.
343 The dykes vary in composition (volatile free) from phonolite to phono-tephrite based
344 on their classification by a SiO_2 versus Zr/Ti diagram modified after Winchester and Floyd
345 (1977) (Fig. 4). Despite being strongly altered, the phono-tephrites are tightly clustered, and
346 plot in between the phono-tephrite fields for Tristan da Cunha alkaline lavas (Le Roex et al.,
347 1990) and the Mt. Vulture lavas (Beccaluva et al., 2002); also shown in Figure 4 are the
348 compositions of the lavas of the Teide-Pico Viejo Volcanic Complex, which overlap those of
349 the Tristan da Cunha field (Ablay et al., 1998). The phonolites define a linear trend of
350 increasing SiO_2 content and Zr/Ti ratios that span the entire phonolite field. The compositions
351 of the nepheline syenites generally overlap those of the phonolites (Fig. 4). However, the
352 contents of SiO_2, Fe_2O_3 and MgO of the phonolite range to higher values than those of the
353 nepheline syenite and the alkali concentrations are lower. The phono-tephrite is characterised
354 by much lower SiO_2, Al_2O_3 and alkali contents than the other two rock-types and is strongly
355 enriched in MgO, CaO and TiO_2 (Table 1). The peralkalinity index of the phonolite and
356 phono-tephrite is lower (0.79 and 0.81, respectively) than that of the nepheline syenite (0.97),
357 due probably to alteration. The Mg number (100*MgO/(MgO+FeO)) decreases from 54.87 in
358 the phono-tephrite to 12.97 in the phonolite and 12.66 in the nepheline syenite.
359 The mantle-normalised REE profiles of the phonolite and phono-tephrite are identical
360 within error (Fig. 3a). In addition, they are parallel to the profiles of the nepheline syenite and
361 carbonatite, however, the REE concentration of the nepheline syenite is much lower and that
362 of the carbonatite is significantly higher; the carbonatite is also more enriched in the LREE
363 (Fig. 3a). The phono-tephrites, phonolites and nepheline syenites are strongly enriched in Nb,
364 Ta, U, Pb, Hf, Zr relative to primitive mantle, evident as positive anomalies on spidergrams,
365 however, the anomalies are strongest for the phonolite. Significantly, the positive anomalies

Bodeving, S., Williams-Jones, A.E., Swinden, S., 2017. Carbonate–silicate melt immiscibility, REE mineralising fluids, and the evolution of the Lofdal Intrusive Suite, Namibia. Lithos 268–271, 383-398. http://dx.doi.org/10.1016/j.lithos.2016.11.024.

for Ba, Ta, Pb, Zr and Hf in the phono-tephrite and phonolite are mirrored by negative anomalies for these elements in the calcio-carbonatite, and the positive anomaly for Sr in calcio-carbonatite is mirrored by a negative anomaly for this element in phono-tephrite and phonolite (Fig. 3b).

The average Y/Ho ratios of the phono-tephrite, the phonolite and the nepheline syenite are, respectively, 29.2, 29.5and 25.9, which is relatively close to the mantle value of 27.4 (supplementary material ESM_2_6a). The corresponding Zr/Hf ratios are 64.3, 80.8 and 80.6, and the Nb/Ta ratios are 17.7, 30.5 and 31.3, respectively (supplementary material ESM_2_6b,c; Table 1).

In comparison to fresh nepheline syenite, the metasomatically altered nepheline syenite (fenite) is strongly enriched in K_2O (10.11 wt.% versus 6.48 wt.%) and marked by a significant loss in Na_2O (2.48 wt.% versus 7.32 wt.%). Moreover, SiO_2 and CaO were enriched during fenitisation, whereas Al_2O_3 and Fe_2O_3 were depleted (Table 1). The REE profiles (Fig. 3c) are identical within error and the trace element profiles, normalised to primitive mantle, (Fig. 3d) are similar except for U, Nb and Pb, which are considerably enriched in the fenites.

7. CARBON AND OXYGEN ISOTOPES

Carbon and oxygen isotopic analyses were performed on calcite in carbonatite from the Main Intrusion, dykes outside it and the breccia infill. They show a limited range of $\delta^{13}C$ values, namely between -4.72 and -6.35 ‰, whereas the range in $\delta^{18}O$ values is considerably greater, from +6.46 to +23.16 ‰ (Fig. 5, Table 2). Most samples form a tight cluster in the mantle box or plot in the overlapping box for primary igneous carbonatite (Taylor et al., 1967; Deines, 1989). Several samples from the Main Intrusion and dykes outside it have much higher $\delta^{18}O$ values, forming a more diffuse group between +18.24 and +23.16 ‰.

Bodeving, S., Williams-Jones, A.E., Swinden, S., 2017. Carbonate–silicate melt immiscibility, REE mineralising fluids, and the evolution of the Lofdal Intrusive Suite, Namibia. Lithos 268–271, 383-398. http://dx.doi.org/10.1016/j.lithos.2016.11.024.

8. DISCUSSION

8.1. Magma source

Most carbonatites and associated silica-undersaturated alkaline silicate rocks form in intracontinental extensional tectonic settings where asthenospheric upwelling, commonly driven by mantle plumes, leads to decompressional melting (Fitton and Upton, 1987; Woolley, 1989). An intracontinental rift setting is also proposed for the Lofdal Intrusive Suite, based on the observation that, within error, it is the same age as the alkali rhyolites of the nearby Naauwpoort Formation, which researchers generally agree, were emplaced during a phase of intracontinental rifting prior to the onset of the Damaran Orogeny (de Kock et al., 2000).

Isotopic support for a mantle origin for the nepheline syenites of the Lofdal Intrusive Suite is provided by low initial $^{87}Sr/^{86}Sr$ and $^{206}Pb/^{204}/Pb$ ratios, and high εNd values (Jung et al., 2007). Further support is provided by the behaviour of the geochemical twins, Y/Ho and Nb/Ta. All of the major silicate igneous units in the Lofdal Intrusive Suite, i.e., phono-tephrite, phonolite, and nepheline syenite have Y/Ho ratios that are close to the mantle value of 27.7; within error, the average values, 25.8, 29.2 and 29.5, respectively, are indistinguishable from the mantle value (supplementary material ESM_2_ 6a; Sun and McDonough, 1989). Only the phono-tephrite has a Nb/Ta ratio close to the mantle value (17.7 versus 17.4; Sun and McDonough, 1989). The higher Nb/Ta values of the phonolite (30.5) and nepheline syenite (31.32) may be explained by the evolution, via fractionation, of the corresponding magmas from a phono-tephrite magma. Somewhat surprisingly, the Zr/Hf ratio of the phono-tephrite (64.3) is considerably higher than the mantle ratio (36.2; Sun and McDonough, 1989), although it is lower than that of the phonolite (80.8) and the nepheline syenite (80.6. However, this is also a feature of some mantle xenoliths and abyssal

Bodeving, S., Williams-Jones, A.E., Swinden, S., 2017. Carbonate–silicate melt immiscibility, REE mineralising fluids, and the evolution of the Lofdal Intrusive Suite, Namibia. Lithos 268–271, 383-398. http://dx.doi.org/10.1016/j.lithos.2016.11.024.

peridotites, and although the reason for the deviation from the mantle value is not well understood, it has been suggested that it may be due to mass-dependent fractionation (Niu, 2004; Huang et al., 2011). Thus, despite having the same charge and ionic radius, the strength of bonds involving Zr will be different from those involving Hf because of the differences in their masses (in principle, the same should be true for Nb and Ta).

Significantly, the Y/Ho ratio for carbonatite, 27.3, is closest to the mantle value. This observation is important because opinion is divided over whether carbonatite magmas originate by direct melting of the mantle (Sweeney, 1994; Harmer and Gittins, 1998; Wyllie and Lee, 1998; Mitchell, 2005; Chakhmouradian, 2006) or evolve from mantle-derived silicate magmas by liquid immiscibility (von Eckermann, 1948; Kjarsgaard and Hamilton, 1989; Gittins, 1989) or fractional crystallisation (King, 1949; Watkinson and Wyllie, 1971; Veksler et al., 1998a). In the case of the evolution of carbonatite magmas from silicate magmas, it has been proposed that this could occur either in the mantle or the crust. Indeed, Woolley and Kjarsgaard (2008) have proposed that carbonatites associated with phonolites (the case at Lofdal) form in the crust from mantle-derived silicate magmas. If this were the case at Lofdal, however, it would be reasonable to expect some disturbance of the Y/Ho ratio due to crustal contamination, for which there is no evidence. Additional, even more compelling support for the formation of the carbonatites in the mantle is provided by oxygen and carbon stable isotope data for calcite from the carbonatite. Most of the data plot directly in the mantle field defined by Taylor (1967) and the remaining data either plot in the immediately adjacent igneous carbonatite field, or have mantle-like carbon isotope signatures, but much higher $\delta^{18}O$ values that we attribute to low temperature interaction with formational waters (Fig. 5); at 100 °C $\Delta^{18}O$ calcite-H_2O is 25‰ and is even greater at lower temperature (O'Neil et al., 1969; Deines, 1989). A little unexpectedly, the carbonatites have much higher average Zr/Hf and Nb/Ta values than primitive mantle (63.6 versus 36.2 and

Bodeving, S., Williams-Jones, A.E., Swinden, S., 2017. Carbonate–silicate melt immiscibility, REE mineralising fluids, and the evolution of the Lofdal Intrusive Suite, Namibia. Lithos 268–271, 383-398. http://dx.doi.org/10.1016/j.lithos.2016.11.024.

352.3 vs 17.4; Sun and McDonough, 1989). However, the Zr/Hf value is very similar to that reported by Chakhmouradian (2006) for carbonatites, which he argues formed by partial melting from an enriched (metasomatised) mantle source. The Nb/Ta ratio is extremely high and contains a very large uncertainty, which may point towards a decoupling of the geochemical pair (Brod et al., 2013). We therefore conclude that, irrespective of how it formed, the Lofdal carbonatite magma was produced in the mantle.

8.2. Evolution of the alkaline silicate magmas

8.2.1. Phono-tephrite – phonolite dykes

Earlier we showed that the composition of the Lofdal silicate dykes varies continuously and linearly from low (phono-tephrite) to high (phonolite) SiO_2 concentration and Zr/Ti ratio (Fig. 4). This suggests a magmatic evolution of phono-tephrite to phonolite, and is consistent with the observation that the phono-tephrites, despite being altered, display a very narrow range in composition, implying that they represent the primitive magma from which the phonolites were derived (the phonolites exhibit a wide range in composition). The latter is also consistent with the observation that only the phono-tephrites have mantle values of the geochemical twin, Nb/Ta (discussed in the previous section); the values of Nb/Ta of the phonolites are much higher. As Si and Zr are incompatible elements and Ti is compatible, we therefore propose that the magmas evolved by fractional crystallisation from phono-tephrite to phonolite and that samples of phonolite with the highest concentration of SiO_2 and highest Zr/Ti ratio represent the most evolved silicate magmas. The fractional crystallisation trend illustrated above is also evident in Harker plots (Figs. 6a, b). Concentrations of the compatible elements, Mg, Fe, Ti and P, decrease from phono-tephrite to phonolite, whereas those of the incompatible elements Al, Si. Na, K, Zr, Hf, Ta, Nb and REE increase (Fig. 6 c,d; Table 1). This reflects the fact that during fractional crystallisation the compatible

Bodeving, S., Williams-Jones, A.E., Swinden, S., 2017. Carbonate–silicate melt immiscibility, REE mineralising fluids, and the evolution of the Lofdal Intrusive Suite, Namibia. Lithos 268–271, 383-398. http://dx.doi.org/10.1016/j.lithos.2016.11.024.

466 elements were depleted by concentrating preferentially in the fractionating minerals and the
467 incompatible elements were concentrated in the residual melt.

468 We modelled the fractional crystallisation to determine if the observed phonolite
469 composition could be derived from a more primitive phono-tephrite melt. This involved
470 changing the initial bulk composition of an assumed primitive magma (average Lofdal
471 phono-tephrite) by fractionating a previously defined mineral assemblage (plagioclase, alkali
472 feldspar, nepheline, diopside, biotite, Ti-bearing magnetite, apatite, and olivine) in 1% steps.
473 After each step, the masses of each element corresponding to the amounts crystallised by
474 each aliquot of minerals was subtracted from the corresponding masses of the hypothetical
475 residual liquid. The proportions of this mineral assemblage were changed until the best fit
476 between the model and bulk compositional data was obtained. As is evident from Figure 7
477 a,b,c,d and Table 3, the model satisfactorily reproduces the observed trends by mainly
478 fractionating K-feldspar and very minor nepheline. Not all elements have distributions that
479 readily illustrate fractional crystallisation. For example, the REE profiles of the phono-
480 tephrite and phonolite, normalised against primitive mantle, are very similar (Fig. 3a). This
481 confirms earlier conclusions that the two rock types are genetically related but suggests that
482 the REE were not significantly fractionated. The primitive mantle-normalised trace-element
483 profiles (spidergrams), however, are much more indicative of the more fractionated state of
484 the phonolites, displaying large enrichments relative to phono-tephrite in incompatible
485 elements like Th, U, Nb, Ta, Pb, Zr, and Hf (Fig. 3b).

486 Three main hypotheses have been proposed for the formation of alkaline silica-
487 undersaturated magmas. The first involves small degrees of partial melting of an enriched
488 metasomatised mantle or lower crust (Sutcliffe et al., 1990; Lubala et al., 1994; Litvinovsky
489 et al., 2002) and the second, the generation of a residual melt by fractional crystallisation
490 from an alkali basalt parental melt (Roex et al., 1990; Thirlwall and Burnard, 1990; Thorpe

Bodeving, S., Williams-Jones, A.E., Swinden, S., 2017. Carbonate–silicate melt immiscibility, REE mineralising fluids, and the evolution of the Lofdal Intrusive Suite, Namibia. Lithos 268–271, 383-398.
http://dx.doi.org/10.1016/j.lithos.2016.11.024.

491 and Tindle, 1992; Foland et al., 1993; Ablay et al., 1998). The third involves mixing of a
492 mafic and a silicic melt, generating hybrid liquids (Brown and Becker, 1986; Zhao et al.,
493 1995; Litvinovsky et al., 2002; Jung et al., 2007). The geochemistry of the alkaline silica-
494 undersatured rocks at Lofdal and their evolution points towards the second hypothesis. As
495 was also shown above, the most primitive alkaline silicate rocks are the phono-tephrites,
496 which have high Ni (134 ppm) and Cr (466 ppm) contents, relatively unevolved trace
497 elements signatures (Fig. 3b), and the highest Mg number of all the silicate rocks at Lofdal
498 (55). These rocks are similar to alkaline basalts and differ from them mainly in their higher
499 Zr/Ti ratios (Fig. 4). Moreover, their mantle origin has already been demonstrated by their
500 ratios of the geochemical twins, Y/Ho and Nb/Ta, and they have a restricted range of
501 compositions. We therefore conclude that the phonolites represent the residues of fractional
502 crystallisation of a phono-tephrite (alkali-basalt) parental melt.
503
504 *8.2.2. Nepheline syenite*
505 The nepheline syenite is miaskitic and represents the plutonic member of the alkaline
506 silica-undersaturated rocks at Lofdal. It consists mainly of K-feldspar, nepheline (mostly
507 altered to cancrinite or locally to sodalite), aegirine, biotite, albite, zircon, magnetite and
508 apatite, and is mineralogically similar to the phonolite. The compositions of the groundmass
509 albite, K-feldspar phenocrysts and cancrinite are also almost identical in the two rock types
510 (supplementary material ESM_1). However, although biotite phenocryst compositions in the
511 nepheline syenite and phonolite form a single trend on the biotite classification diagram
512 (supplementary material ESM_2_3), those in the phonolite are more enriched in Fe. The
513 bulk-rock content of SiO_2 and the Zr/Ti ratio also range to higher values in the phonolite (Fig.
514 4). The above observations suggest that the nepheline syenite crystallised from the magma
515 that crystallised the phonolite dykes and that this magma continued to evolve (by crystal

Bodeving, S., Williams-Jones, A.E., Swinden, S., 2017. Carbonate–silicate melt immiscibility, REE mineralising fluids, and the evolution of the Lofdal Intrusive Suite, Namibia. Lithos 268–271, 383-398. http://dx.doi.org/10.1016/j.lithos.2016.11.024.

fractionation) after emplacement of the nepheline syenite, leading to the intrusion of phonolites with much higher SiO_2 contents and Zr/Ti ratios. This interpretation is consistent with the greater similarity of the primitive mantle-normalised trace element profile for nepheline syenite to that of phonolite than to the profile for phono-tephrite (Figs. 3b, d). We therefore conclude that the nepheline syenite (and phonolite) was derived by fractional crystallisation from a primitive phono-tephrite magma.

Application of the nepheline-kalsilite-quartz geothermometer to nepheline phenocrysts suggests that the nepheline syenite crystallised at temperatures between 500°C and 750°C (Fig. 8), assuming compositions in the $NaAlSiO_4$-$KAlSiO_4$-SiO_2-H_2O system (Hamilton and Mackenzie, 1960; Hamilton, 1961). The corresponding average composition of the nepheline is $Ne_{73,68}Ks_{22,07}Qz_{4,26}$, which is consistent with that of a slowly cooled plutonic body, as it plots in the associated Buerger-Morozewicz convergence field. This field represents the compositional range of nepheline in association with microcline or albite in gradually cooled plutonic rocks (Blancher et al., 2010), and is limited by the ideal composition of nepheline ($Ne_{75}Ks_{25}Qz_0$) (Buerger, 1954) and the composition of naturally occurring nepheline ($Ne_{73}Ks_{18}Qz_9$) (Morozewicz, 1928).

A conspicuous feature of the nepheline syenite is that it has a lower REE content than both the phonolite and phono-tephrite, although the primitive mantle-normalised REE profiles of the three rock-types have very similar shapes (Fig. 3a). The reason for this depletion of the REE is not known. However, given the evidence of crystal settling (section 4.1), it seems likely that it was caused by fractional crystallisation of a REE-enriched mineral. The only plausible candidate is pyrochlore, which contains between 2.3 and 2.9 wt.% total REE oxides. The other minerals with significant REE are fluorapatite, which contains <0.5 wt% total REE oxides and zircon, which contains < 0.2 wt.% total REE oxides. However, fluorapatite can be ruled out because the nepheline syenite is enriched in P relative

Bodeving, S., Williams-Jones, A.E., Swinden, S., 2017. Carbonate–silicate melt immiscibility, REE mineralising fluids, and the evolution of the Lofdal Intrusive Suite, Namibia. Lithos 268–271, 383-398. http://dx.doi.org/10.1016/j.lithos.2016.11.024.

to phonolite, and the very low REE content of zircon and low bulk rock Zr content make zircon a very unlikely candidate. We therefore propose that pyrochlore sequestered the REE and settled under gravity in the lower, unexposed part of the intrusion. This would have left the upper parts of the nepheline syenite depleted in REE, thereby explaining why its primitive mantle-normalised REE profile is significantly lower than that of the phonolite, which is interpreted to have formed from the same magma.

As noted in the preceding paragraph, the nepheline syenite bodies, i.e., the Main Intrusion and the two satellite bodies, likely underwent post-emplacement fractional crystallisation. In addition to the behaviour of the REE, the fractionation is also evident in an increased degree of silica-undersaturation from the rim to the centre of the intrusions (the proportion of nepheline increases inwards), with nepheline transforming from an interstitial to a euhedral phenocryst phase. This may suggest that the central parts of the intrusions represent crystal cumulates, as has been proposed for some nepheline syenites (e.g., Eby et al., 1998), and also may help explain some of the compositional differences between the nepheline syenites and the phonolites.

8.3. Carbonatite Genesis

As discussed earlier, the geochemical data presented in this paper provide strong evidence that the carbonatite magma originated in the mantle. Here we evaluate whether it formed as a result of a small degree of partial melting of a metasomatised (including carbonate-altered) mantle, fractional crystallisation of a phono-tephrite magma or by separating as an immiscible liquid from either the phono-tephrite or phonolite magma.

Most studies invoking the formation of a carbonatite magma by partial melting of a CO_2-bearing mantle peridotite (harzburgite or lherzolite) have concluded that the resulting carbonatite will be alkali-rich and dolomitic in composition (Wallace and Green, 1988;

Bodeving, S., Williams-Jones, A.E., Swinden, S., 2017. Carbonate–silicate melt immiscibility, REE mineralising fluids, and the evolution of the Lofdal Intrusive Suite, Namibia. Lithos 268–271, 383-398.
http://dx.doi.org/10.1016/j.lithos.2016.11.024.

566 Sweeney, 1994; Wyllie and Lee, 1998; Lee and Wyllie, 1998b, 2000). These studies were
567 based on experiments at high pressure (>2 GPa). It is possible, however, to generate
568 carbonatites with high values of Ca/(Ca+Mg), i.e., alkali-bearing calcio-carbonatites, at lower
569 pressure. For example, experiments of Dalton and Wood (1993) at 1.5 GPa yielded a calcio-
570 carbonatite with a Ca/(Ca+Mg) value of 0.88 (the corresponding value for the Lofdal calcio-
571 carbonatite is ~0.91). It also has been proposed that calcio-carbonatites can be produced by
572 interaction of a rising magnesio-carbonatite magma with harzburgite or lherzolite, forming
573 wehrlite (Sweeney, 1994; Harmer and Gittins, 1997; Wyllie and Lee, 1998; Lee and Wyllie,
574 2000). Irrespective of whether the calcio-carbonatite forms as a result of partial melting at
575 low pressure or from reaction of magnesio-carbonatite with harzburgite or wehrlite, it will
576 have elevated contents of elements like Ni and Cr, which are concentrated in the latter rocks.
577 In contrast, the Lofdal calcio-carbonatite has contents of these elements below or close to the
578 detection limit, respectively (Table 1). In view of these observations, we therefore conclude
579 that the Lofdal calcio-carbonatites did not originate by direct partial melting of the mantle.
580 An alternative to direct partial melting of the mantle for the generation of carbonatite
581 magmas is fractional crystallisation of a coexisting CO_2-enriched silicate magma (Watkinson
582 and Wyllie, 1971; Kjarsgaard, 1998; Veksler et al., 1998a). In the case of Lofdal, such an
583 alternative would be consistent with the close spatial association of the calcio-carbonatite and
584 alkaline silicate rocks. According to this hypothesis, the calcio-carbonatite would represent
585 the last and smallest volume of residual liquid produced by fractional crystallisation of the
586 phono-tephrite magma (earlier we showed that phono-tephrite is the most primitive of the
587 silicate rocks at Lofdal). The observations that the volume of calcio-carbonatite is relatively
588 small and that calcio-carbonatite intruded the nepheline syenite (Figs. 1, 2a) support this
589 hypothesis. Further support is provided by the behaviour of the REE, which being
590 incompatible are expected to accumulate in the residual liquid. Indeed, the REE

Bodeving, S., Williams-Jones, A.E., Swinden, S., 2017. Carbonate–silicate melt immiscibility, REE mineralising fluids, and the evolution of the Lofdal Intrusive Suite, Namibia. Lithos 268–271, 383-398.
http://dx.doi.org/10.1016/j.lithos.2016.11.024.

591 concentrations are higher in the carbonatite than in the silicate rocks (Fig. 3a). Moreover,
592 there is a systematic increase in the La/Lu ratio from the phono-tephrite (146.3), through the
593 phonolite (155.3) to the carbonatite (288.1), in agreement with the greater size and thus
594 greater incompatibility of the La ion. However, this behaviour is not matched by that of some
595 of the other incompatible elements, notably Ta, Zr and Hf. Whereas, Ta, Zr and Hf are
596 enriched in the phono-tephrite and phonolite, they are depleted in the calcio-carbonatite (Fig.
597 3b). This is a concern. Another concern is the lack of rock-types in the Lofdal Intrusive Suite
598 with compositions intermediate between those of the most evolved phonolite and calcio-
599 carbonatite. Potential problems with the model itself are that the solubility of CO_2 in silicate
600 melts may be too low to precipitate carbonate minerals and that, in competition with SiO_2 and
601 Al_2O_3, Ca, Mg and Fe are unlikely to bond preferentially with CO_2 (Gittins, 1989). Gittins
602 (1989) and Halama et al. (2005) also noted that as clinopyroxene is commonly an early
603 crystallising mineral in the silicate magma, it will remove CaO (and MgO and FeO) making
604 it even more difficult for the magma to evolve to calcio-carbonatite. Clinopyroxene is the
605 main mafic mineral at Lofdal, and although it is present mainly as aegirine/aegirine-augite, its
606 crystallisation would have removed some of the CaO needed to develop a residual calcio-
607 carbonatite liquid. For the above reasons, we therefore conclude it unlikely that the calcio-
608 carbonatite was generated by fractional crystallisation of a silicate (phono-tephrite) magma.
609 The remaining hypothesis for the generation of carbonatite magma is carbonate-
610 silicate liquid immiscibility (von Eckermann, 1948; Kjarsgaard and Hamilton, 1988; Le Bas,
611 1989; Veksler et al., 1998b, 2012; Martin et al., 2013; Weidendorfer et al., 2016). As is the
612 case for the fractional crystallisation hypothesis, the close spatial association of the calcio-
613 carbonatite with silica-undersaturated rocks makes this hypothesis attractive. One of the ways
614 of testing the hypothesis, in principle, the best way barring the discovery of coexisting
615 silicate and carbonate melt inclusions (not found at Lofdal), is to compare the concentration

Bodeving, S., Williams-Jones, A.E., Swinden, S., 2017. Carbonate–silicate melt immiscibility, REE mineralising fluids, and the evolution of the Lofdal Intrusive Suite, Namibia. Lithos 268–271, 383-398.
http://dx.doi.org/10.1016/j.lithos.2016.11.024.

ratios of a suite of elements in related silicate igneous rocks and carbonatites to the corresponding melt partition coefficients for these elements. Although a number of experimental studies have determined coefficients for the partitioning of elements between immiscible carbonate and silicate melts, the most comprehensive studies are those of Veksler et al., (2012) and Martin et al., (2013). These studies show that the partition coefficients vary considerably with melt composition.

We selected partition coefficients determined from four hydrous experiments in which the immiscible silicate melt was closest in composition to the Lofdal phono-tephrites (LM75 and LM113 from Martin et al., 2013; RQ-21 from Veksler et al., 2012) and phonolites (LM73 from Martin et al., 2013). However, all of the melts, both silicate and carbonate, in these experiments (and experiments from other studies), were alkali-rich compared to the Lofdal melts and the carbonate melts contained only half the CaO concentration of the Lofdal calcio-carbonatite; the Lofdal carbonatite likely lost a considerable proportion of Na and K through the release of fenitising fluids, (Table 1). Despite this compositional difference, the element partition coefficients ($D^{Carb/Sil}$) from LM75, LM113, and RQ-21 yield spidergram and REE profiles that are very similar in form to those of the Lofdal calcio-carbonatite/phono-tephrite and calcio-carbonatite/phonolite element ratios, although the absolute values vary considerably (Figs. 9a, b). Thus, on the spidergram (Fig. 9a), troughs in the calcio-carbonatite/phono-tephrite and calcio-carbonatite/phonolite ratios for Zr, Hf, Pb and Ta, are matched by troughs in the corresponding ($D^{Carb/Sil}$) values. The same is true for the peaks in the ratios for Ba, La, Ce. The only exception is the peak in the ratio for Sr, which is not matched by a peak in the ($D^{Carb/Sil}$) values of LM75 and LM113, although it is by a peak in the ($D^{Carb/Sil}$) value for RQ-21. The match of the profile for LM73, which was selected to represent calcio-carbonatite/phonolite partitioning, is not as good. The experimentally determined partition coefficients are much higher, there is no trough for Hf,

Bodeving, S., Williams-Jones, A.E., Swinden, S., 2017. Carbonate–silicate melt immiscibility, REE mineralising fluids, and the evolution of the Lofdal Intrusive Suite, Namibia. Lithos 268–271, 383-398.
http://dx.doi.org/10.1016/j.lithos.2016.11.024.

and there are peaks instead of troughs for Pb and Ta. The profiles for the ($D^{Carb/Sil}$)REE values from LM75, LM113 and LM 73 are all roughly parallel to the profiles of the calcio-carbonatite/phono-tephrite and calcio-carbonatite/phonolite REE ratios, sloping gently downwards from La to Lu, whereas that for the ($D^{Carb/Sil}$) REE values for RQ-21 has a somewhat stronger slope (Fig. 9b). Overall, ($D^{Carb/Sil}$) REE values from experiments LM75 and LM113 most closely match the calcio-carbonatite/phono-tephrite and calcio-carbonatite/phonolite on both the spidergram and REE diagram (Figs. 9a, b)

The remarkable similarity in the shapes of the ($D^{Carb/Sil}$) spidergram profiles and the slopes of the REE profiles to those of the calcio-carbonatite/phono-tephrite and calcio-carbonatite/phonolite element ratios suggests that the Lofdal calcio-carbonatite separated from a silicate magma. Indeed, the match is comparable to that for other carbonatites for which an origin by liquid immiscibility has been proposed (e.g., Doroshkevich et al., 2010; Martin et al., 2012). The hypothesis also explains why incompatible elements like Ta, Zr and Hf are depleted in the calcio-carbonatite relative to the silicate rocks and why the chemical ratios, Nb/Ta and Zr/Hf, of the calcio-carbonatite are much higher and higher, respectively, than the corresponding mantle values; Ta and Hf prefer the silicate magma more than their twins (Bühn and Trumbull, 2003; Brod et al., 2013). Finally, the hypothesis helps explain why the calcio-carbonatite and the silicate rocks at Lofdal have a similar phenocryst mineralogy (supplementary material ESM_1).

In summary, the available evidence appears to rule out an origin for the calcio-carbonatites by partial melting of mantle, and suggests that it is unlikely that they were the product of simple fractional crystallisation. By contrast, the evidence is satisfactorily explained by separation of a carbonatite liquid from a phono-tephrite magma or its evolved phonolitic counterpart.

Bodeving, S., Williams-Jones, A.E., Swinden, S., 2017. Carbonate–silicate melt immiscibility, REE mineralising fluids, and the evolution of the Lofdal Intrusive Suite, Namibia. Lithos 268–271, 383-398.
http://dx.doi.org/10.1016/j.lithos.2016.11.024.

8.4. Fenitisation

A process commonly accompanying the emplacement of carbonatite intrusions is the hydrothermal alteration of the country rock by alkaline metasomatic fluids exsolved from the carbonatite magma (Morogan and Woolley, 1988; Williams-Jones and Palmer, 2002; Le Bas, 2008). At Lofdal, the loss of Na and gain in K suggest that the fenitisation was potassic. Field and petrographic observations support this interpretation. The protolith, nepheline syenite, was gradually altered in an aureole around the intruding calcio-carbonatite. Adjacent to the contact, there was almost complete recrystallisation of the K-feldspar to microcline. Biotite, nepheline, cancrinite and aegirine were replaced by microcline, calcite, lesser albite and apatite. This change in mineralogy is reflected in a loss in Na, Fe and Al and a significant gain in K (Table 1; supplementary material ESM_2_8). The trace elements U, Nb and Pb, experienced a strong enrichment (Fig. 3d, Table 1).

In addition to fenitising the nepheline syenite, carbo-hydrothermal fluids released from the carbonatite magma are also considered to have been responsible for the diatreme breccias observed along the margins of the Main Intrusion. These fluids likely accumulated at the top of the magma chamber, building up pressure on the adjacent wallrock, and were released explosively to form the diatreme breccias. Support for this interpretation is provided by the carbonate matrix, which has been shown to have a mantle carbon and oxygen isotopic composition (Fig. 5), i.e., to have originated from a calcio-carbonatite magma.

8.5. Source of the REE mineralising fluids

The REE mineralisation, which is currently the target of exploration, comprises an indicated mineral resource of 2.88 Mt grading 0.32 wt.% total REE oxides, of which 76.3% is heavy REE oxides, and an inferred mineral resource of 3.28 Mt grading 0.27 wt.% total REE oxides, of which 74.7% is heavy REE oxides, at a cut-of grade of 0.1 wt.% total REE oxides

Bodeving, S., Williams-Jones, A.E., Swinden, S., 2017. Carbonate–silicate melt immiscibility, REE mineralising fluids, and the evolution of the Lofdal Intrusive Suite, Namibia. Lithos 268–271, 383-398. http://dx.doi.org/10.1016/j.lithos.2016.11.024.

691 (www.namibiarareearths.com). This extreme heavy REE oxide enrichment is surprising as
692 REE mineralisation associated with carbonatites is typically dominated by LREE (Pell,
693 1996). The mineralisation is hosted in brecciated and carbonated albitised structures
694 following the main regional foliation in the basement; the calcio-carbonatite contains no
695 economic REE mineralisation.

696 Although the Lofdal calcio-carbonatite displays similar LREE enrichment to other
697 carbonatites (e.g., Alnö, Fen, Phalaborwa, Sokli, Silinjärvi and Kaiserstuhl; Hornig-
698 Kjarsgaard, 1998), the REE profiles of the latter are strongly depleted in the HREE, whereas
699 the Lofdal carbonatites have profiles that are flat from Gd to Lu (Fig. 10). Relative to other
700 carbonatites, the Lofdal calcio-carbonatite is thus HREE enriched. As the calcio-carbonatites
701 have the highest REE content (including HREE) of any primary igneous rock at Lofdal and
702 the partition coefficients for the REE between aqueous fluid and carbonatite are greater than
703 for the REE between aqueous fluid and peralkaline silicate magmas (Martin et al., 2013;
704 Song et al., 2016), we therefore propose that the calcio-carbonatite magma was the source of
705 the REE. We envisage, as do Wollenberg et al. (in prep), that the REE were transported in
706 carbo-hydrothermal fluids released from a carbonatite magma and travelled up faults in the
707 basement, where they preferentially concentrated the less mobile HREE allowing the more
708 mobile LREE to leave the system (Williams-Jones et al., 2012; Migdisov and Williams-
709 Jones, 2014).

710

711 **9. PETROGENETIC MODEL**

712 On the basis of its age and tectonic relationship to the alkali rhyolites of the
713 Naauwpoort Formation, we propose that the Lofdal Intrusive Suite was emplaced during the
714 intracontinental rifting that preceded amalgamation of Gondwana and the onset of the
715 Damaran Orogeny. We also propose, on the basis of trace element geochemistry and carbon

Bodeving, S., Williams-Jones, A.E., Swinden, S., 2017. Carbonate–silicate melt immiscibility, REE mineralising fluids, and the evolution of the Lofdal Intrusive Suite, Namibia. Lithos 268–271, 383-398. http://dx.doi.org/10.1016/j.lithos.2016.11.024.

716 and oxygen isotopic compositions (carbonatite) that the corresponding magmas originated in
717 the mantle (Figs. 3a, b and 5).

718 The major and trace element data show that the phono-tephrite, phonolite, nepheline
719 syenite and calcio-carbonatite were all co-genetic, that the phono-tephrite was the most
720 primitive of these magmas, and that the subsequent magmatic evolution lead to the formation
721 of phonolite and nepheline syenite (Figs. 3, 4, 6, supplementary material ESM_2). Based on
722 the bulk rock composition, and a simple fractionation model, we propose that early crystal
723 fractionation, mostly of K-feldspar and very minor nepheline, from the phono-tephrite
724 magma lead to the formation of a phonolite magma enriched in incompatible elements (Fig.
725 7). This magma gave rise to the nepheline syenites of the Main Intrusion and its satellites, as
726 well as the phonolite dykes.

727 After consideration of the data, and particularly a comparison of the profiles of the
728 ratios of trace elements in calcio-carbonatite and silicate rocks to experimentally determined
729 element partition coefficients for coexisting silicate and carbonate liquids, we conclude that
730 separation of carbonate magma as an immiscible liquid from a silicate magma best explains
731 the genesis of the calcio-carbonatite (Figs. 9a, b). The data do not allow us to establish
732 definitively whether this magma was the primitive magma that gave rise to the phono-tephrite
733 dykes or the more evolved magma that produced the phonolites and nepheline syenite.
734 However, as the phono-tephrite dykes contain almost twice as much Ca as the phonolite
735 dykes, it seems more likely that the calcio-carbonatite separated from the phono-tephrite
736 magma than the phonolite magma. Irrespective of whether the source of the calcio-
737 carbonatite was a phono-tephrite or phonolite magma, the only hypothesis that offers a
738 reasonable explanation for the relative depletion of Ta, Zr and Hf in the calcio-carbonatite is
739 carbonate-silicate liquid immiscibility.

Bodeving, S., Williams-Jones, A.E., Swinden, S., 2017. Carbonate–silicate melt immiscibility, REE mineralising fluids, and the evolution of the Lofdal Intrusive Suite, Namibia. Lithos 268–271, 383-398.
http://dx.doi.org/10.1016/j.lithos.2016.11.024.

The exsolved carbonate melt was rich in volatiles (also incompatible) and alkalis, and forcibly intruded into the nepheline syenite, forming calcio-carbonatite and releasing carbo-hydrothermal fluids that fenitised the adjacent host rock. Locally, these fluids also produced diatreme breccias. The fenitisation enriched the nepheline syenite in K, LREE, U, Nb, Ta, Pb, Mo, Zr and Hf (Table 1). The carbonate magma was also injected into the adjacent gneisses where it formed calcio-carbonatite dykes and released fluids that fenitised the gneisses.

The origin of the HREE mineralisation, which is hosted in brecciated and carbonated albitites that cut the gneisses and is currently being explored, is still unclear. However, as the carbonatites have the highest concentration of the REE of any of the igneous rock types observed at Lofdal (they also partition the REE into aqueous fluids more strongly than silicate magmas), and differ from other carbonatites described in the literature in having unusually high concentrations of HREE, they would seem to be the most likely source for the REE. We consider that the REE were released from a calcio-carbonatite magma into carbo-hydrothermal fluids that travelled up faults in the basement, where they preferentially deposited the less mobile HREE as xenotime-(Y).

ACKNOWLEDGEMENTS

The research was funded by a grant from Namibia Rare Earths Inc. and a matching grant from the NSERC Collaborative and Development program. Don Burton, President of Namibia Rare Earths Inc. proposed the project, arranged the necessary logistical support and provided access to the property, drill core and company data. Rowan Wollenberg and company geologists, Bonniface Katanga, Gideon K. Haingura, and Freddy AC. Muyamba assisted in the field work. Shi Lang helped with the electron microprobe analyses, Galen Halverson made his isotope laboratory available for the carbon and oxygen isotopic analyses, and Caitlin Beland provided an Excel program for modelling fractional crystallisation. The

765 manuscript benefitted considerably from constructive reviews by Adrian Finch and two
766 anonymous referees, and helpful comments from Editor-in Chief, Nelson Eby.
767

Bodeving, S., Williams-Jones, A.E., Swinden, S., 2017. Carbonate–silicate melt immiscibility, REE mineralising fluids, and the evolution of the Lofdal Intrusive Suite, Namibia. Lithos 268–271, 383-398.
http://dx.doi.org/10.1016/j.lithos.2016.11.024.

768 **REFERENCES**

769 Ablay, G.J., Carroll, M.R., Palmer, M.R., Martí, J., Sparks, R.S.J. (1998). Basanite-Phonolite
770 Lineages of the Teide-Pico Viejo Volcanic Complex, Tenerife, Canary Islands. Journal
771 of Petrology 39, 905-936.

772 Beccaluva, L., Coltorti, M., Girolamo, P.Di., Melluso, L., Milani, L., Morra, V., Siena, F.
773 (2002). Petrogenesis and evolution of Mt. Vulture alkaline volcanism (Southern Italy).
774 Mineralogy and Petrology 74, 277-297.

775 Blancher, S.B., D'Arco, P., Fonteilles, M., Pascal, M.-L. (2010). Evolution of nepheline from
776 mafic to highly differentiated members of the alkaline series: the Messum complex,
777 Namibia. Mineralogical Magazine 74, 415-432.

778 Brod, J.A., Junqueira-Brod, T.C., Gaspar, J.C., Petrinovic, I.A., de Castro Valente, S.,
779 Corval, A. (2013). Decoupling of paired elements, crossover REE patterns, and mirrored
780 spider diagrams: Fingerprinting liquid immiscibility in the Tapira alkaline-carbonatite
781 complex, SE Brazil. Journal of South American Earth Sciences 41, 41-56.

782 Brown, P.E., Becker, S.M. (1986). Fractionation, hybridisation and magma-mixing in the
783 Kialineq centre East Greenland. Contributions to Mineralogy and Petrology 92, 57-70.

784 Buerger, M.J. (1954). The stuffed derivatives of the silica structures. American Mineralogist
785 39, 600-614.

786 Bühn, B. & Trumbull, R.B. (2003). Comparison of petrogenetic signatures between mantle-
787 derived alkali silicate intrusives with and without associated carbonatite, Namibia. Lithos
788 66, 201-221.

789 Chakhmouradian, A.R. (2006). High-field-strength elements in carbonatitic rocks:
790 Geochemistry, crystal chemistry and significance for constraining the sources of
791 carbonatites. Chemical Geology 253, 138-160.

792 Dalton, J.A. & Presnall, D.C. (1998). The Contiuum of Primary Carbonatitic-Kimberlitic
793 Melt Compositions in Quilibrium with Lherzolite: Data from the System CaO-MgO-
794 Al2O3-SiO2-CO2 at 6 GPa. Journal of Petrology 39, 1953-1964.
795 Dalton, J.A. & Wood, B.J. (1993). The composition of primary carbonate melts and their
796 evolution through wallrock reaction in the mantle. Earth and Planetary Science Letters
797 119, 511-525.
798 Dasgupta, R. & Hirschmann, M.M. (2007). A modified interactive sandwich method for
799 determination of near-solidus partial melt compositions. II. Application to determination
800 of near-solidus melt compositions of carbonated peridotite. Contributions to Mineralogy
801 and Petrology 154 (6), 647-661.
802 Dasgupta, R., Hirschmann, M.M., McDonough W.F., Spiegelman, M., Withers, C. (2009).
803 Trace element portioning between garnet lherzolite and carbonatite at 6.6. and 8.6 GPa
804 with applications to the geochemistry of the mantle and mantle-derived melts. Chemical
805 Geology 262 (1-2), 57-77.
806 Deines, P. (1989). Stable isotope variations in carbonatites. In: Bell, K. (Eds.), Carbonatites:
807 Genesis and Evolution. Unwin Hyman, London, pp 301-359.
808 de Kock, G.S., Eglington, B., Armstrong, R.A., Harmer, R.E., Walraven, F. (2000). U-Pb and
809 Pb-Pb ages of the Naauwpoort rhyolite, Kawakeup leptite and Okongava Diorite:
810 implications for the onset of rifting and of oogenesis in the Damara belt, Namibia.
811 Communications of the Geological Survey of Namibia 12, 89-97.
812 Do Cabo, V.N. (2014). Geological, mineralogical and geochemical characterization of the
813 Heavy Rare Earth-rich carbonatites at Lofdal, Namibia. PhD Thesis Camborne School of
814 Mines, University of Exeter.

Bodeving, S., Williams-Jones, A.E., Swinden, S., 2017. Carbonate–silicate melt immiscibility, REE mineralising fluids, and the evolution of the Lofdal Intrusive Suite, Namibia. Lithos 268–271, 383-398.
http://dx.doi.org/10.1016/j.lithos.2016.11.024.

815 Doroshkevich, A.G., Ripp, G.S., Moore, K.R. (2010). Genesis of the Khaluta alkaline-basic
816 Ba-Sr carbonatite complex (West Transbaikala, Russia). Mineralogy and Petrology 98,
817 245-268.
818 Duncan, R. A., Hooper, P. R., Rehacek,, J.,. Marsh J. S., Duncan, A. R. (1997). The timing
819 and duration of the Karoo igneous event, southern Gondwana. Journal of Geophysical
820 Research 102, 18127–18138.
821 Eby, G.N., Woolley, A.R., Din, V., Platt, G. (1998). Geochemistry and petrogenesis of
822 nepheline syenites: Kasungu-Chipala, Ilomba, and Ulindi nepheline syenite intrusions,
823 North Nyasa Alkaline Province, Malawi. Journal of Petrology, 39, 1405-1424.
824 Fitton, J.G. & Upton, B.G.J. (1987). Introduction: Alkaline Igneous Rocks – In Fitton, J.G.,
825 Upton, B.G.J. (Eds.), Alkaline Igneous Rocks. Geological Society Special Publication
826 30, 1-545.
827 Foland, K.A., Landoll, J.D., Henderson, C.M.B., Jiangfeng, C. (1993). Formation of
828 cogenetic quartz and nepheline syenites. Geochimica et Cosmochimica Acta 57, 697-
829 704.
830 Frets, D.C. (1969). The Geology and Structure of the Huab-Welwitschia Area South West
831 Africa. Chamber of Mines Precambrian Research Unit, University of Cape Town,
832 Bulletin 5, 1-235.
833 Gaudet, M. (2013). Mineralogical Study of Uranium and Niobium Mineralization at the Main
834 Intrusion of the Lofdal Carbonatite Complex, Namibia, Africa. B Sc Thesis Dalhousie
835 University.
836 Ghosh, S., Ohtani, E., Litasov, K.D., Terasaki, H. (2009). Solidus of carbonated peridotite
837 from 10-20 GPa and origin of magnesiocarbonatite melt in the Earth's deep mantle.
838 Chemical Geology 262, 17-28.

839 Gittins, J. (1989). The origin and evolution of carbonatite. In: Bell, K. (Eds.), Carbonatites:
840 Genesis and Evolution. Unwin Hyman, London, pp 580-599.
841 Gittins, J., Harmer, R.E. (1997). What is ferrocarbonatite? A revised classification. Journal of
842 African Earth Sciences 25, 189-168.
843 Gray, D.R., Foster, D.A., Meert, J.G., Goscombe, B.D., Armstrong, R., Trouw, R.A.J.,
844 Passcier, C.W. (2008). A Damara orogen perspective on the assembly of southwestern
845 Gondwana. Journal of the Geological Society of London Special Publication 294, 257-
846 278.
847 Gudfinnsson, G.H., Presnall, D.C. (2005). Continous Gradations among Primary
848 Carbonatitic, Kimberlitic, Melilitic, Basaltic, Picritic and Komatiitic Melts in
849 Equilibrium with Garnet Lherzolite at 3-8GPa. Journal of Petrology 46, 1645-1659.
850 Halama, R., Vennemann, T., Siebel, W., Markl, G. (2005). The Grønnedal-Ika Carbonatite-
851 Syenite Complex, South Greenland: Carbonatite Formation by Liquid Immiscibility.
852 Journal of Petrology 46, 191-217.
853 Hamilton, D.L. (1961). Nepheline as crystallization temperature indicators. Journal of
854 Geology 69, 321-329.
855 Hamilton, D.L., MacKenzie, W.S. (1960). Nepheline solid solution in the system $NaAlSiO_4$-
856 $KAlSiO_4$-SiO_2. Journal of Petrology 1, 56-72.
857 Harmer, R.E., Gittins, J. (1997). The origin of dolomitic carbonatites: field and experimental
858 constraints. Journal of African Earth Sciences 25, 5-28.
859 Harmer, R.E., Gittins, J. (1998). The case for primary, mantle-derived carbonatite magma.
860 Journal of Petrology 39, 1895-1903.
861 Hoffman, P.F., Hawkins, D.P., Isachsen, C.E., Bowring, S.A. (1996). Precise U-Pb zircon
862 ages for early Damaran magmatism in the Summas Mountains and Welwitschia Inlier,
863 northern Damara belt. Communications of the Geological Survey of Namibia 11, 47–52.

Bodeving, S., Williams-Jones, A.E., Swinden, S., 2017. Carbonate–silicate melt immiscibility, REE mineralising fluids, and the evolution of the Lofdal Intrusive Suite, Namibia. Lithos 268–271, 383-398. http://dx.doi.org/10.1016/j.lithos.2016.11.024.

Hornig-Kjarsgaard, I. (1998). Rare Earth Elements in Sövitic Carbonatites and their Mineral Phases. Journal of Petrology 39, 2105-2121.

Huang, H., Niu, Y., Zhidan, Z., Huixin, H., Dicheng, Z. (2011). On the enigma of Nb-Ta and Zr-Hf fractionation – a critical review. Journal of Earth Sciences 22, 52-66.

Jung, S., Hoffer, E., Hoernes, S. (2007). Neo-Proterozoic rift-related syenites (Northern Damara Belt, Namibia): Geochemical and Nd–Sr–Pb–O isotope constraints for mantle sources and petrogenesis. Lithos 96, 514-435.

King, B.C. (1949). The Napak area of Karamoja, Uganda. Geological Survey of Uganda, Memoir V pp. 57.

Kjarsgaard, B.A., Hamilton, D.L. (1988). Liquid immiscibility and the origin of alkali-poor carbonatites. Mineralogical Magazine 52, 43-55.

Kjarsgaard, B.A., Hamilton, D.L. (1989). The genesis of carbonatites by immiscibility. In: Bell, K. (Eds.), Carbonatites: Genesis and Evolution. Unwin Hyman, London, pp 388-403.

Kjarsgaard, B.A., Hamilton, D.L., Peterson, T.D. (1995). Peralkaline nephelinite/carbonatite liquid immiscibility: comparison of phase compisitions in experiments and natural lavas from Oldoinyp Lengai. In: Bell, K., Keller, J. (Eds.), Carbonatite Volcanism: Oldoinyo Lengai and Petrogenesis of Natrocarbonatites. Springer Verlag, Berlin, pp 4-22.

Kjarsgaard, B.A. (1998). Phase relations of a Carbonated High-CaO Nephelinite at 0.2 and 0.5 GPa. Journal of Petrology 39 (11-12), 2061-2075.

Le Bas, M.J. (1989). Diversification of carbonatite. In: Bell, K. (Eds.), Carbonatites: Genesis and Evolution. Unwin Hyman, London, pp 105-141.

Le Bas, M.J. (2008). Fenites associated with carbonatites. The Canadian Mineralogist 46, 915-932.

888 Lee, W.J., Wyllie, P.J. (1994). Experimental Data Bearing on Liquid Immiscibility, Crystal
889 Fractionation, and the Origin of Calciocarbonatites and Natrocarbonatites. International
890 Geology Review 36, 797-819.
891 Lee, W.J., Wyllie, P.J. (1998a). Petrogenesis of carbonatite magmas from mantle to crust,
892 constrained by the system CaO-(MgO+FeO*)–(Na_2O + K_2O)–(SiO_2 + Al_2O_3 + TiO_2)-
893 CO_2 Journal of Petrology 39, 495-517.
894 Lee, W.J., Wyllie, P.J. (1998b). Processes of Crustal Carbonatite Formation by Liquid
895 Immiscibility and Differentiation, Elucidated by Model Systems. Journal of Petrology
896 39, 2005-2013.
897 Lee, W.J., Wyllie, P.J. (2000). The system CaO-MgO-SiO_2-CO_2 at 1 GPa, metasomatic
898 wehrlites, and primary carbonatite magmas. Contributions to Mineralogy and Petrology
899 138, 214-228.
900 Le Roex, A.P., Cliff, R.A., Adair, B.J.I.A. (1990). Tristan da Cunha, South Atlantic:
901 geochemistry and petrogenesis of a Basanite-Phonolite Lava Series. Journal of Petrology
902 31, 779-812.
903 Litvinovsky, B.A., Jahn, B.M., Zanvilevich, A.N., Shadaev, M.G. (2002). Crystal
904 fractionation in the petrogenesis of an alkali monzodiorite-syenite series: the Oshurkovo
905 plutonic sheeted complex, Transbaikalia, Russia. Lithos 64, 97-130.
906 Lubala, R.T., Frick, C., Roders, J.H., Walraven, F. (1994). Petrogenesis of syenites and
907 granites of the Schiel Alkaline complex, Northern Transvaal, South Africa. Journal of
908 Geology 102, 307-316.
909 Martin, L.H.J., Schmidt, M.W., Mattsson, H.B., Guenther, D. (2013). Element portioning
910 between Immiscible Carbonatite and Silicate Melts for Dry and H2O-bearing System at
911 1.3 GPa. Journal of Petrology 54, 2301-2338.

Bodeving, S., Williams-Jones, A.E., Swinden, S., 2017. Carbonate–silicate melt immiscibility, REE mineralising fluids, and the evolution of the Lofdal Intrusive Suite, Namibia. Lithos 268–271, 383-398.
http://dx.doi.org/10.1016/j.lithos.2016.11.024.

912 Martin, L.H.J., Schmidt, M.W., Mattsson, H.B., Ulmer, P., Hametner, K., Günther, D.
913 (2012). Element portioning between immiscible carbonatite-kamafugite melts with
914 application to the Italian ultrapotassic suite. Chemical Geology 320-321, 96-112.
915 Migdisov, A.A., Williams-Jones, A.E. (2014). Hydrothermal transport and deposition of the
916 rare earth elements by fluorine-bearing aqueous liquids. Mineralium Deposita 49 (8),
917 987-997.
918 Migdisov, A.A., Williams-Jones, A.E., Wagner, T. (2009). An experimental study of the
919 solublity and speciation of the Rare Earth Elements (III) in fluoride- and chloride-
920 bearing aqueous solutions at temperatues up to 300°C. Geochimica et Cosmochimica
921 Acta 73, 7087-7109.
922 Miller, R.M. (2008). Neoproterozoic and early Paleozoic Rocks of the Damara Orogen. In:
923 Miller, R.M. (Eds.), The Geology of Namibia. Geological Survey Windhoek, pp 13-1-
924 14-1.
925 Mitchell, R.H. (2005). Carbonatites carbonatites and carbonatites. The Canadian Mineralogist
926 43, 2049-2068.
927 Morogan, V., Woolley, A.R. (1988). Fenitzation at the Alnö carbonatite complex, Sweden;
928 distribution, mineralogy and genesis. Contributions to Mineralogy and Petrology 100,
929 169-182.
930 Morozewicz, J. (1928). Über die chemische zusammensetzung des gesteinsbildenenden
931 nephelins. Fennia 22, 1-16.
932 Niu, Y. (2004). Bulk rock major and trace element compositions of abyssal peridotite:
933 implications for mantle melting, melt extraction and post-melting processes beneath mid-
934 ocean ridges. Journal of Petrology 45, 2423-2458.
935 O'Neil, J.R., Clayton, R.N., Mayeda, T.K. (1969). Oxygen isotope fractionation in divalent
936 metal carbonates. Journal of Chemical Physics 51, 5547-5558.

937 Pell, J. (1996). Mineral Deposits associated with carbonatites and related alkaline igneous
938 rocks - In Mitchell, R.R. (Eds.), Undersaturated alkaline rocks: mineralogy, petrogenesis,
939 and economic potential. Mineralogical Association of Canada, Short Course Series,
940 Winnipeg, pp 271-310.
941 Porada, H. (1989). Pan-African Rifting and Orogenesis in Southern to Equatorial Africa and
942 Eastern Brazil. Precambrian Research 44, 103-136.
943 Rieder, M., Cavazzini, G., D'Yakonov, Y.S., Frank-Kamenetskii, V.A., Gottardi, G.,
944 Guggenheim, S., Koval, P.V., Müller, G., Neiva, A.M.R., Radoslovich, E.W., Robert, J-
945 L., Sassi, F.P., Takeda, H., Weiss, Z., and Wones, D.R. (1998). Nomenclature of the
946 micas. The Canadian Mineralogist 36, 905-912.
947 Song, W.l., Xu, C., Veksler, I.V., Kynicky, J. (2016). Experimental study of REE, Ba, Sr, Mo
948 and W partitioning between carbonatitic melt and aqueous fluid with implicaions for rare
949 metal mineraliazion. Contributions to Mineralogy and Petrology 171 (1), 1-12.
950 Sun, S.S., McDonough, W.F. (1989). Chemical and isotopic systematics of oceanic basalts:
951 implications for mantle composition and processes. The Journal of the Geological
952 Society of London Special Publication 42, 313-345.
953 Sutcliffe, R.H., Smith, A.R., Doherty, W., Barnett, R.L. (1990). Mantle derivation of Archean
954 amphibole-bearing granitoid and associated mafic rocks: evidence from the Superior
955 Province, Canada. Contributions to Mineralogy and Petrology 105, 255-274.
956 Sweeney, R.J. (1994). Carbonatite melt compositions in the Earth's mantle. Earth and
957 Planetary Science Letters 128, 259-270.
958 Taylor, H.P., Frechen, J.J., Degens, E.T. (1967). Oxygen and carbon isotope studies of
959 carbonatites from the Laacher See District, West Germany and the Alnö District,
960 Sweden. Geochimica et Cosmochimica Acta 31, 407-430.

Bodeving, S., Williams-Jones, A.E., Swinden, S., 2017. Carbonate–silicate melt immiscibility, REE mineralising fluids, and the evolution of the Lofdal Intrusive Suite, Namibia. Lithos 268–271, 383-398.
http://dx.doi.org/10.1016/j.lithos.2016.11.024.

961 Thirlwall, M.F., Burnardm P. (1990). Pb-Sr-Nd isotope and chemical study of the origin of
962 undersatured and oversatured shoshonitic magmas from the Borralan pluton, Assynt,
963 NW Scotland. The Journal of the Geological Society of London 147, 259-269.
964 Thorpe, R.S., Tindle, A.G. (1992). Petrology and petrogenesis of a tertiary bimodal dolerite-
965 peralkaline/subalkaline trachyte/rhyolite dyke association from Lundy, Bristol Channel,
966 UK. Geological Journal 27, 101–117.
967 Veksler, I.V., Dorfman, A.M., Dulski, P., Kamenetsky, V.S., Danyushevsky, L.V., Jeffries,
968 T., Dingwell, D.B. (2012). (2012) Partitioning of elements between silicate melt and
969 immiscible fluoride, chloride, carbonate, phosphate and sulphate melts, with implications
970 to the origin of natrocarbonatite. Geochimica et Cosmochimica Acta 79, 20-40.
971 Veksler, I.V., Nielsen, T.F.D., Sokolov, S.V. (1998a). Mineralogy of Crystallized Melt
972 Inclusions from Gardiner and Kovdor Ultramafic Alkaline Complexes: Implications for
973 Carbonatite Genesis. Journal of Petrology 39, 2015-2031.
974 Veksler, I.V., Petibon, C., Jenner, G.A., Dorfman, A.M., Dingwell, D.B. (1998b). Trace
975 Element Partitioning in Immiscible Silicate-Carbonate Liquid Systems: an Initial
976 Experimental Study Using a Centrifuge Autoclave. Journal of Petrology 39, 2095-2104.
977 von Eckermann, H. (1948). The alkaline district of Alnö Island. Sveriges geol. Undersök.
978 Ser. Ca 36, 1–176.
979 Wall, F., Niku-Paalova, V.N., Storey, C., Müller, A., Jeffries, T. (2008). Xenotime-(Y) from
980 carbonatite dykes at Lofdal, Namibia: Unusually low LREE:HREE ratio in carbonatite,
981 and the first dating of xenotime overgrowth on zircon. The Canadian Mineralogist 46,
982 861-877.
983 Wallace, M.E., Green, D.H. (1988). An experimental determination of primary carbonatite
984 magma composition. Letters to Nature 335, 343-346.

Bodeving, S., Williams-Jones, A.E., Swinden, S., 2017. Carbonate–silicate melt immiscibility, REE mineralising fluids, and the evolution of the Lofdal Intrusive Suite, Namibia. Lithos 268–271, 383-398.
http://dx.doi.org/10.1016/j.lithos.2016.11.024.

985 Watkinson, D.H., Wyllie, P.J. (1971). Experimental Study of the Composition Join
986 $NaAlSiO_4$-$CaCO_3$-H_2O and the Genesis of Alkalic Rock-Carbonatite Complexes. Journal
987 of Petrology 12, 357-378.
988 Weidendorfer, D., Schmidt, M.W., Mattsson, H.B. (2016). Fractional crystallization of Si-
989 undersaturated alkaline magmas leading to unmixing of carbonatites on Brava Island
990 (Cape Verde) and a general model of carbonatite genesis in alkaline magma suites.
991 Contributions to Mineralogy and Petrology 171 (5), 1-29.
992 Wilkinson, J.F.G., Hensel, H.D. (1994). Nephelines and analcimes in some alkaline igneous
993 rocks. Contributions to Mineralogy and Petrology 118, 79-91.
994 Williams-Jones, A.E., Migdisov, A.A., Samson, I.M. (2012). Hydrothermal Mobilisation of
995 the Rare Earth Elements – a tale of "Ceria" and "Yttria". Elements 8, 355-360.
996 Williams-Jones, A.E., Palmer, D.A.S. (2002). The evolution of aqueous-carbonic fluids in the
997 Amba Dongar carbonatite, India: implications for fenitisation. Chemical Geology 185,
998 283-301.
999 Winchester, J.A., Floyd, P.A. (1977). Geochemical discrimination of different magma series
1000 and their differentiation products using immobile elements. Chemical Geology 20, 325-
1001 343.
1002 Woolley, A.R. (1989). The spatial and temporal distribution of carbonatites. In: Bell, K.
1003 (Eds.), Carbonatites: Genesis and Evolution. Unwin Hyman, London, pp 15-34.
1004 Woolley, A.R., Kjarsgaard, B.A. (2008). Paragenetic types of carbonatite as indicated by the
1005 diversity and relative abundances of associated silicate rocks: Evidence from a global
1006 database. The Canadian Mineralogist 46, 741-752.
1007 Wyllie, P.J., Lee, W.J. (1998). Model System Controls on Conditions for Formation of
1008 Magnesiocarbonatite and Calciocarbonatite Magmas from the Mantle. Journal of
1009 Petrology 39, 1885-1893.

Bodeving, S., Williams-Jones, A.E., Swinden, S., 2017. Carbonate–silicate melt immiscibility, REE mineralising fluids, and the evolution of the Lofdal Intrusive Suite, Namibia. Lithos 268–271, 383-398. http://dx.doi.org/10.1016/j.lithos.2016.11.024.

1010 Wyllie, P.J., Tuttle, O.F. (1960). The system $CaO-CO_2-H_2O$ and the origin of carbonatites.
1011 Journal of Petrology 1, 1-46.
1012 Zhao, J.X., Shiraishi, K., Sheraton, J.W. (1995). Geochemical and isotopic studies of syenites
1013 from the Yamato Mountains, East Antarctica: Implications for the origin of syenitic
1014 magmas. Geochimica et Cosmochimica Acta 59, 1363-1382.
1015

Bodeving, S., Williams-Jones, A.E., Swinden, S., 2017. Carbonate–silicate melt immiscibility, REE mineralising fluids, and the evolution of the Lofdal Intrusive Suite, Namibia. Lithos 268–271, 383-398.
http://dx.doi.org/10.1016/j.lithos.2016.11.024.

FIGURE CAPTIONS

Fig. 1 Geological map of the Lofdal Intrusive Suite (Datum WGS84, Zone 33S) (Namibia Rare Earths Inc., 2015) (overview map modified after Gray et al., 2008). Carbonatite and phonolite/phono-tephrite dykes are represented as dark brown and red lines on the map, respectively.

Fig. 2 a. Carbonatite (light grey) intruded into nepheline syenite in the Main Intrusion. b. Small carbonatite dyke (dark brown) intruded into nepheline syenite and surrounded by fenite (light reddish brown). Unaltered nepheline syenite (grey) can be seen in the background. c. Diatreme breccia containing variably-sized rounded fragments cemented by carbonate. d. Amygdaloidal phono-tephrite in contact with phonolite dyke (top, pink). Both are folded.

Fig. 3 a. Primitive mantle-normalised rare earth element profiles of the average calcio-carbonatite, phonolite, phono-tephrite, and nepheline syenite. b. Primitive mantle-normalised trace element profiles (spidergrams) of the average calcio-carbonatite, phonolite and phono-tephrite. c. Primitive mantle-normalised rare earth element profiles of the average nepheline syenite and fenite. d. Primitive mantle-normalised trace element profiles (spidergrams) of the average nepheline syenite and fenite. The vertical bars illustrate the standard deviation for each element. The primitive mantle values are from Sun and McDonough (1989).

Fig. 4 Compositions of the phonolite, phono-tephrite and nepheline syenite on a modified version of the SiO_2 versus Zr/Ti classification diagram of Winchester and Floyd (1977). Compositions of phono-tephrite from the Tristan da Cunha alkaline lava series (TdC) (Le Roex et al., 1990), the Mt. Vulture lava series (MV) (Beccaluva et al., 2002) and the Teide-Pico Viejo Volcanic Complex (TPV) (Ablay et al., 1998) are shown for comparison. They plot in the original basanite-trachybasanite-nephelinite field of Winchester and Floyd (1977),

Bodeving, S., Williams-Jones, A.E., Swinden, S., 2017. Carbonate–silicate melt immiscibility, REE mineralising fluids, and the evolution of the Lofdal Intrusive Suite, Namibia. Lithos 268–271, 383-398.
http://dx.doi.org/10.1016/j.lithos.2016.11.024.

which we have accordingly renamed the phono-tephrite field. The data have been corrected for loss on ignition (LOI).

Fig. 5 Carbon and oxygen isotopic compositions of calcio-carbonatite from the Main Intrusion, dykes and the breccia matrix. The fields of mantle (MTL) and primary igneous carbonatite (CAR) were taken from Taylor et al. (1967) and Deines (1989)

Fig. 6 Harker diagrams showing the distribution in phono-tephrite and phonolite of a. Fe_2O_3(T)+MnO versus SiO_2. b. TiO_2 versus SiO_2. c. Na_2O+K_2O versus SiO_2. d. Al_2O_3 versus SiO_2

Fig. 7 Binary oxide plots (mol.%) showing the predicted trends of fractional crystallisation for phonolite, modelled from the starting composition of an average phono-tephrite (green lines), compared to analysed phonolite compositions (purple symbols; the dashed purple lines represent least squares fits to the data). a. SiO_2 versus Na_2O+K_2O b. MgO versus Al_2O_3 c. TiO_2 versus Al_2O_3 d. SiO_2 versus P_2O_5. Details of the model are provided in the text and Table 3

Fig. 8 Composition of nepheline from two samples of nepheline syenite, NLOFDR3353 and NLOFDR3356, projected onto a nepheline-kalsilite-quartz diagram calibrated for temperature using the data of Hamilton and Mackenzie (1960), Hamilton (1961) and Wilkinson and Hensel (1994). The points M and B represent the Morozewicz natural nepheline composition ($Ne_{73}Ks_{18}Qz_9$) and the Buerger ideal nepheline composition ($Ne_{75}Ks_{25}Qz_0$)

Fig. 9 a. Carbonatite-phono-tephrite and carbonatite-phonolite ratios for a selection of trace elements compared to experimentally determined carbonate-silicate partition coefficients profiles for these elements in hydrous melts from Veksler et al. 2012 (RQ-21) and Martin et al. 2013 (LM75, LM113, LM73). b. Carbonatite-phono-tephrite and carbonatite-phonolite

Bodeving, S., Williams-Jones, A.E., Swinden, S., 2017. Carbonate–silicate melt immiscibility, REE mineralising fluids, and the evolution of the Lofdal Intrusive Suite, Namibia. Lithos 268–271, 383-398.
http://dx.doi.org/10.1016/j.lithos.2016.11.024.

ratios of the rare earth elements compared to experimentally determined carbonate-silicate partition coefficients profiles for these elements in hydrous melts from Veksler et al. 2012 (RQ-21) and Martin et al. 2013 (LM75, LM113, LM73)

Fig. 10 Primitive mantle-normalised rare earth element profiles of the Lofdal calcio-carbonatite compared with those of carbonatites from Oka, Alnö, Fen, Phalaborwa, Sokli, Silinjärvi and Kaiserstuhl (Hornig-Kjaarsgard, 1998). (Primitive mantle values are from Sun and McDonough, 1989)

Bodeving, S., Williams-Jones, A.E., Swinden, S., 2017. Carbonate–silicate melt immiscibility, REE mineralising fluids, and the evolution of the Lofdal Intrusive Suite, Namibia. Lithos 268–271, 383-398.
http://dx.doi.org/10.1016/j.lithos.2016.11.024.

1071 **TABLES**

1072 **Table 1:** Average compositions of the different members of the Lofdal Intrusive Suite

1073 **Table 2:** Oxygen and carbon isotope ratios for calcite in the carbonatite

1074 **Table 3:** Fractional Crystallisation Model

Bodeving, S., Williams-Jones, A.E., Swinden, S., 2017. Carbonate–silicate melt immiscibility, REE mineralising fluids, and the evolution of the Lofdal Intrusive Suite, Namibia. Lithos 268–271, 383-398. http://dx.doi.org/10.1016/j.lithos.2016.11.024.

SUPPLEMENTARY MATERIAL

ESM-1.xls

Sample list and GPS points; whole rock data of calcio-carbonatite, phono-tephrite, phonolite, nepheline syenite, fenite and whole rock standards and blank data; electron microprobe mineral chemical data for calcite, feldspar, nepheline, cancrinite, biotite, clinopyroxene, zircon, apatite and pyrochlore (Gaudet 2012); electron microprobe standards.

ESM-2.pdf

1. Microphotographs in cross-polarised light (a,b,d). Microphotograph in polarised light (c). a. A euhedral nepheline phenocryst with a cancrinite (cc) reaction rim (NLOFDR3356), euhedral titanite (ti) and biotite (bt) and aegirine (ae) in nepheline syenite. b. Euhedral apatite (ap) crystals in nepheline syenite. c. A euhedral, zoned pyrochlore (py) crystal surrounded by aegirine (ae) with adjacent apatite (ap) and calcite (ca) in calcio-carbonatite. d. K-feldspar (K-fs) phenocrysts (sanidine?) in phonolite that have been variably altered to microcline (mc), surrounded by a fine-grained matrix of biotite (bt), albite (ab) and K-feldspar.

2. The composition of feldspar in nepheline syenite, fenite, calcio-carbonatite and phonolite plotted on the feldspar ternary classification diagram modified after Schairer (1950) in terms of the components albite (Ab), orthoclase (Or) and anorthite (An). Note: ANO = anorthosite, SAN = sanidine, OLI = oligoclase, AND = andesine, LAB = labradorite, BYT = bytownite.

3. Composition of the Lofdal mica plotted on the biotite classification diagram of Rieder *et al.* (1998).

Bodeving, S., Williams-Jones, A.E., Swinden, S., 2017. Carbonate–silicate melt immiscibility, REE mineralising fluids, and the evolution of the Lofdal Intrusive Suite, Namibia. Lithos 268–271, 383-398.
http://dx.doi.org/10.1016/j.lithos.2016.11.024.

4. Clinopyroxene composition in nepheline syenite and calcio-carbonatite phenocrysts illustrated on the classification ternary for sodic pyroxenes (after Morimoto; 1989). Quad (Q) represents wollastonite, enstatite and ferrosilite of the Mg-Ca-Fe group of pyroxenes.

5. The range of carbonatite compositions illustrated on the carbonatite classification diagram of Gittins and Harmer (1997).

5. Composition of the Lofdal nepheline syenite on the plutonic Total-Alkali-Silica diagram of Wilson (1989).

6. a. A binary plot showing the concentration of Y versus that of Ho in bulk rock samples of the phono-tephrites, phonolites, nepheline syenites and carbonatites. The trend-line represents the mantle value of approximately 27.7 (Sun and McDonough, 1989). b. A binary plot showing the concentration of Nb versus that of Ta in bulk rock samples of the phono-tephrites, phonolites, nepheline syenites and carbonatites. The trend-line represents the mantle value of approximately 17.4 (Sun and McDonough, 1989). c. A binary plot showing the concentration of Zr versus that of Hf in bulk rock samples of the phono-tephrites, phonolites, nepheline syenites and carbonatites. The trend-line represents the mantle value of approximately 36.2 (Sun and McDonough, 1989).

7. A binary plot showing the concentration of K_2O versus Na_2O in nepheline syenite and fenite.

Bodeving, S., Williams-Jones, A.E., Swinden, S., 2017. Carbonate–silicate melt immiscibility, REE mineralising fluids, and the evolution of the Lofdal Intrusive Suite, Namibia. Lithos 268–271, 383-398.
http://dx.doi.org/10.1016/j.lithos.2016.11.024.

Figure 1

Click here to download high resolution image

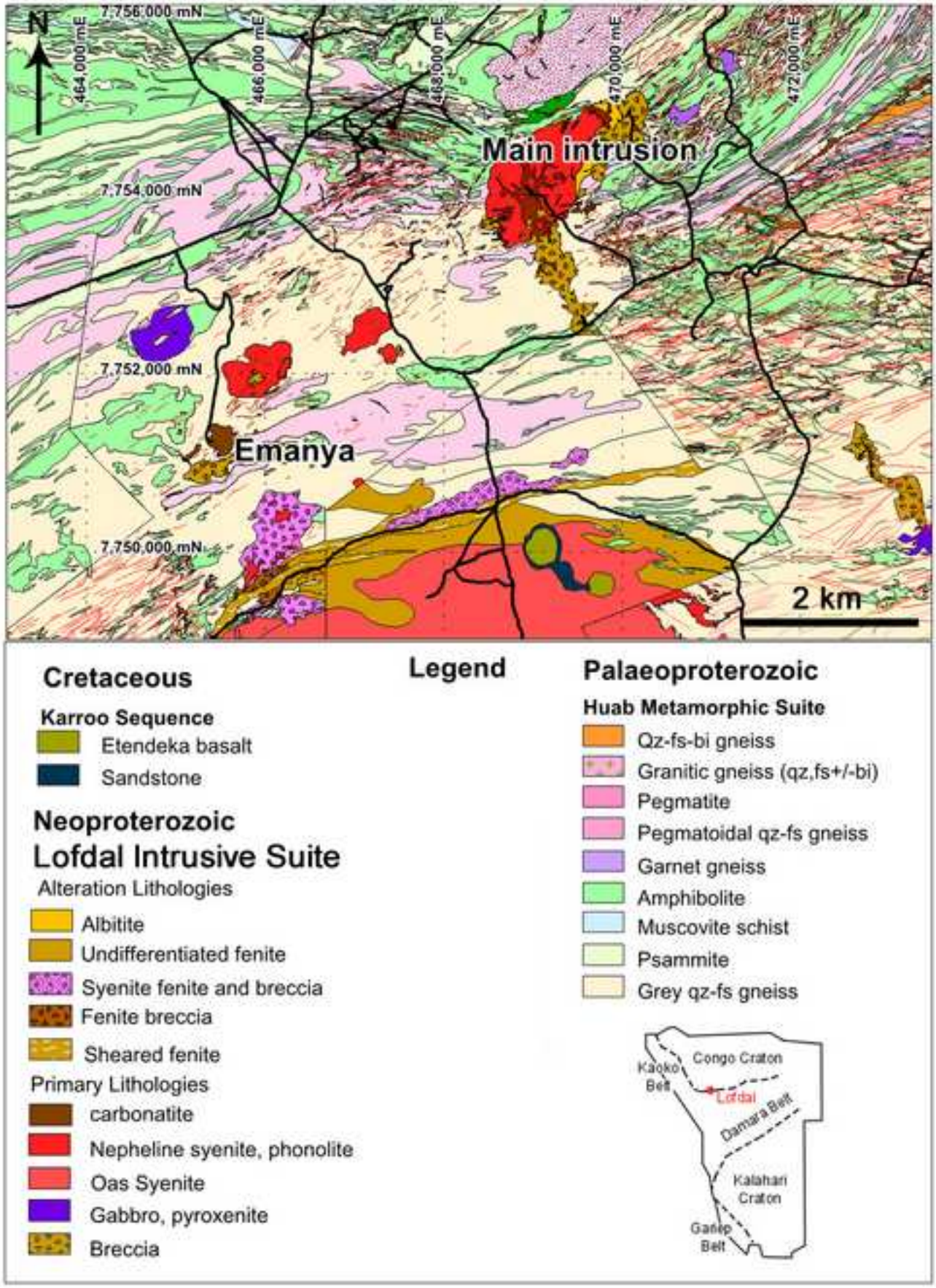

Bodeving, S., Williams-Jones, A.E., Swinden, S., 2017. Carbonate–silicate melt immiscibility, REE mineralising fluids, and the evolution of the Lofdal Intrusive Suite, Namibia. Lithos 268–271, 383-398. http://dx.doi.org/10.1016/j.lithos.2016.11.024.

Figure 2a

Click here to download high resolution image

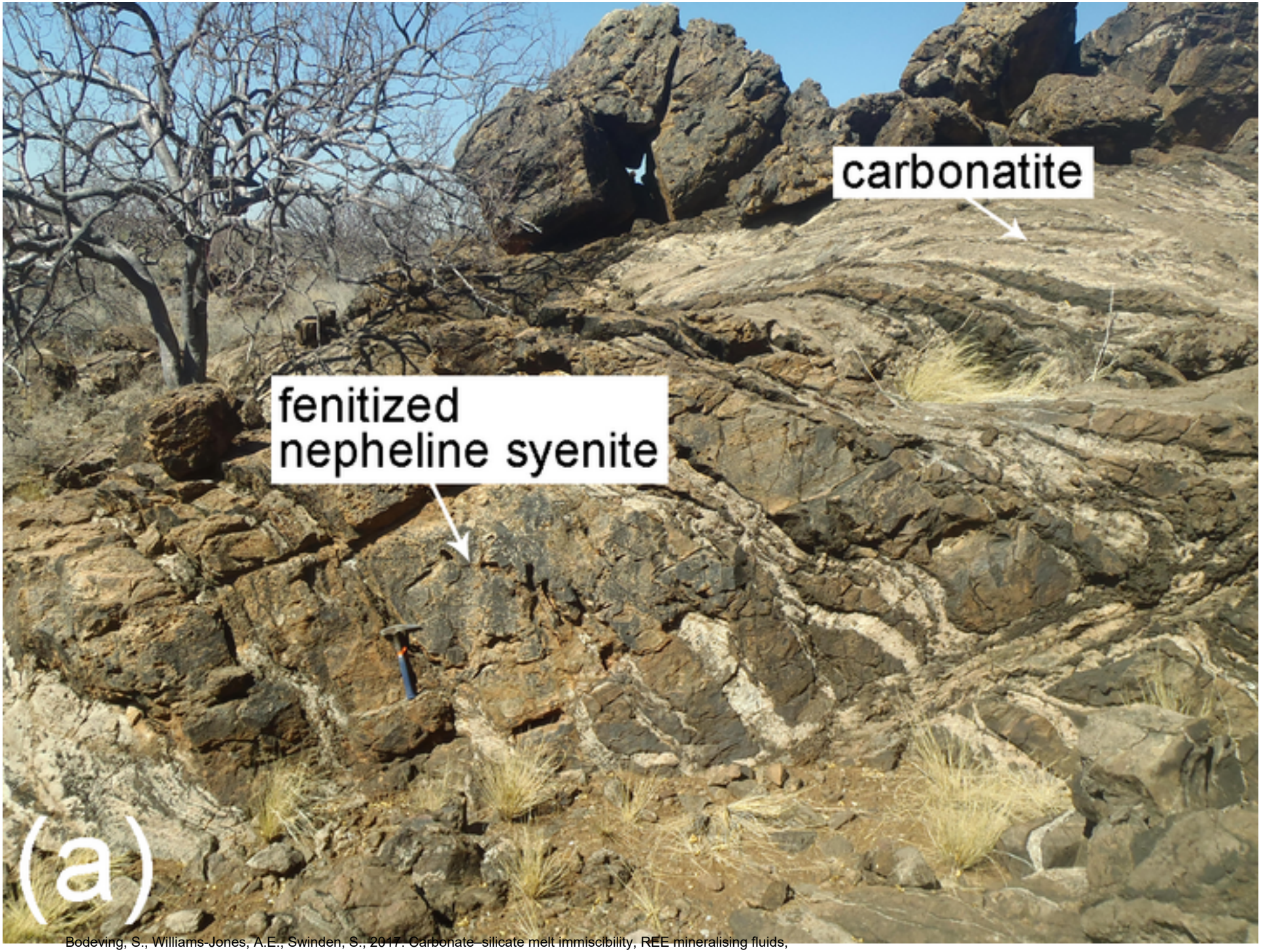

Bodeving, S., Williams-Jones, A.E., Swinden, S., 2017. Carbonate–silicate melt immiscibility, REE mineralising fluids, and the evolution of the Lofdal Intrusive Suite, Namibia. Lithos 268–271, 383-398. http://dx.doi.org/10.1016/j.lithos.2016.11.024.

Figure 2b

Click here to download high resolution image

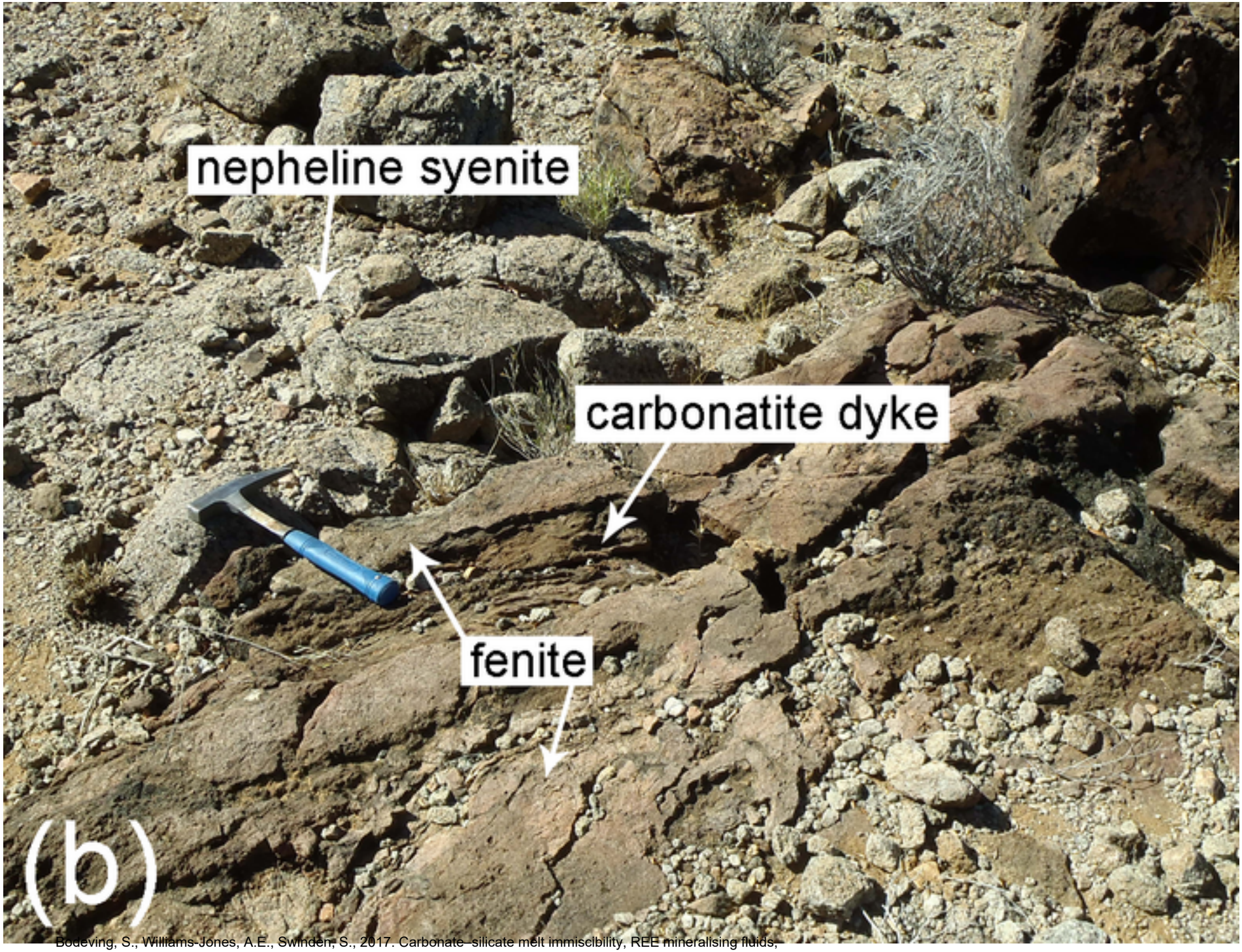

Bodeving, S., Williams-Jones, A.E., Swinden, S., 2017. Carbonate–silicate melt immiscibility, REE mineralising fluids, and the evolution of the Lofdal Intrusive Suite, Namibia. Lithos 268–271, 383-398. http://dx.doi.org/10.1016/j.lithos.2016.11.024.

Figure 2c
Click here to download high resolution image

Bodeving, S., Williams-Jones, A.E., Swinden, S., 2017. Carbonate–silicate melt immiscibility, REE mineralising fluids, and the evolution of the Lofdal Intrusive Suite, Namibia. Lithos 268–271, 383-398. http://dx.doi.org/10.1016/j.lithos.2016.11.024.

Figure 2d

Click here to download high resolution image

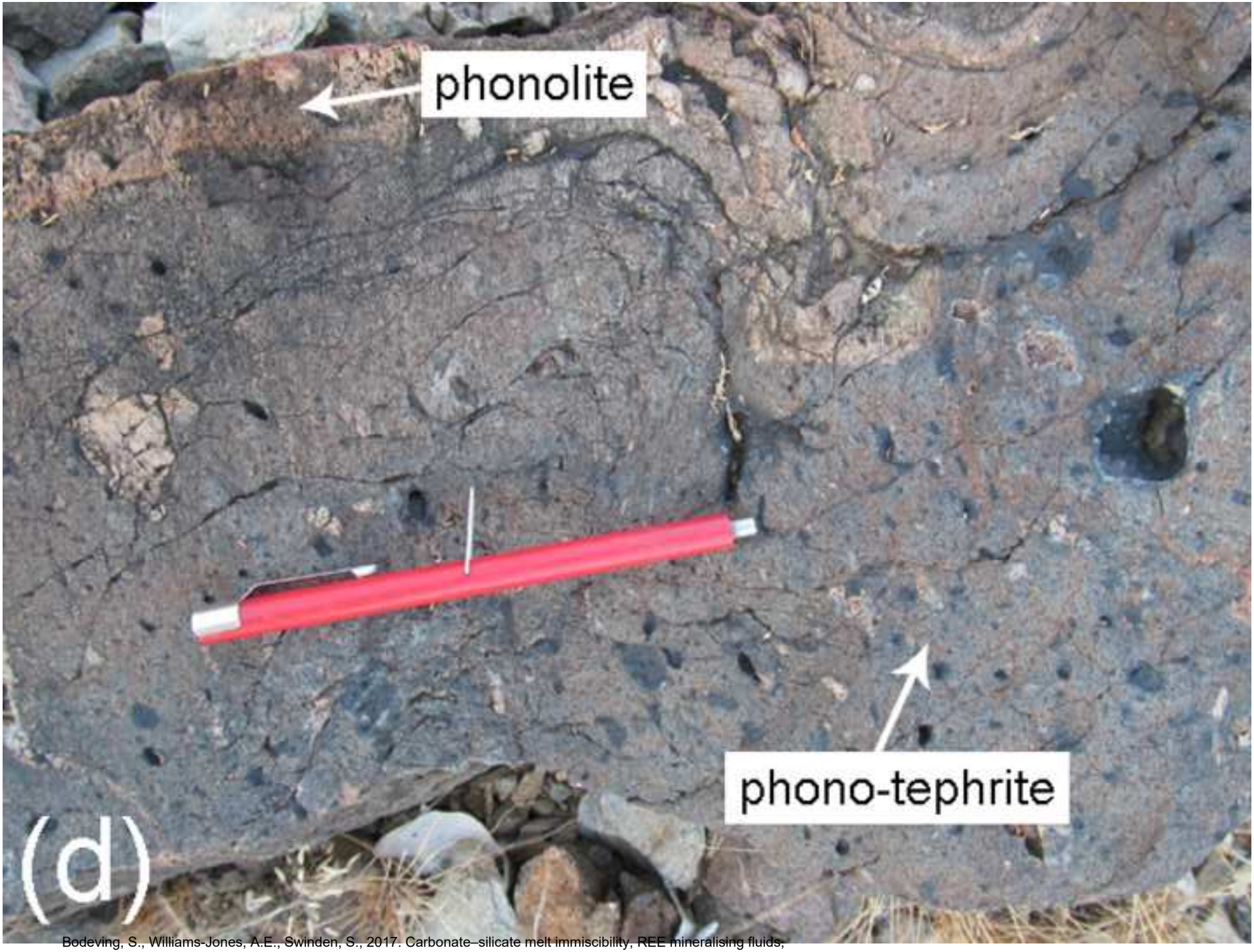

Bodeving, S., Williams-Jones, A.E., Swinden, S., 2017. Carbonate–silicate melt immiscibility, REE mineralising fluids, and the evolution of the Lofdal Intrusive Suite, Namibia. Lithos 268–271, 383-398. http://dx.doi.org/10.1016/j.lithos.2016.11.024.

Figure 3a

Click here to download high resolution image

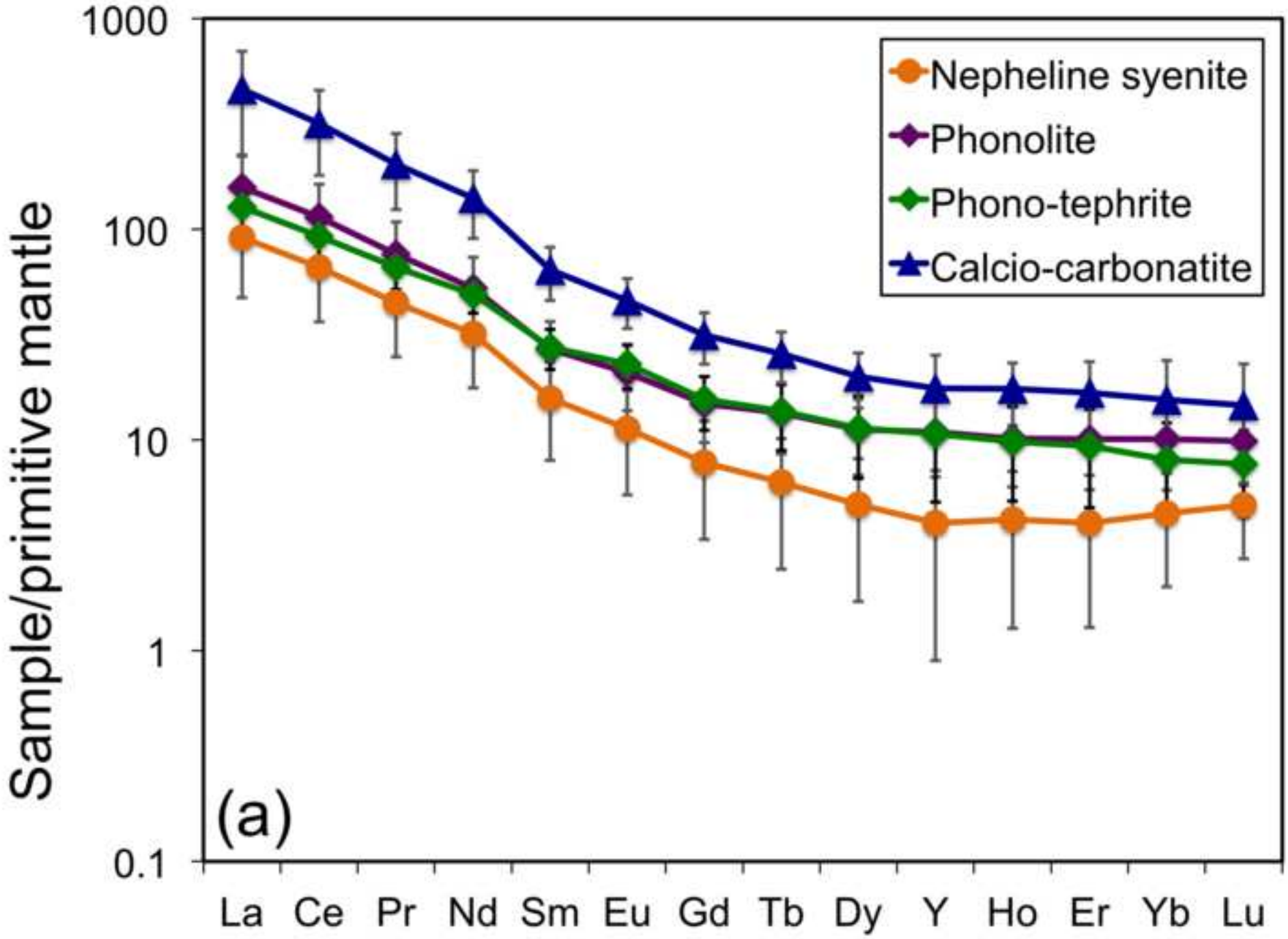

Bodeving, S., Williams-Jones, A.E., Swinden, S., 2017. Carbonate–silicate melt immiscibility, REE mineralising fluids, and the evolution of the Lofdal Intrusive Suite, Namibia. Lithos 268–271, 383-398. http://dx.doi.org/10.1016/j.lithos.2016.11.024.

Figure 3b

Click here to download high resolution image

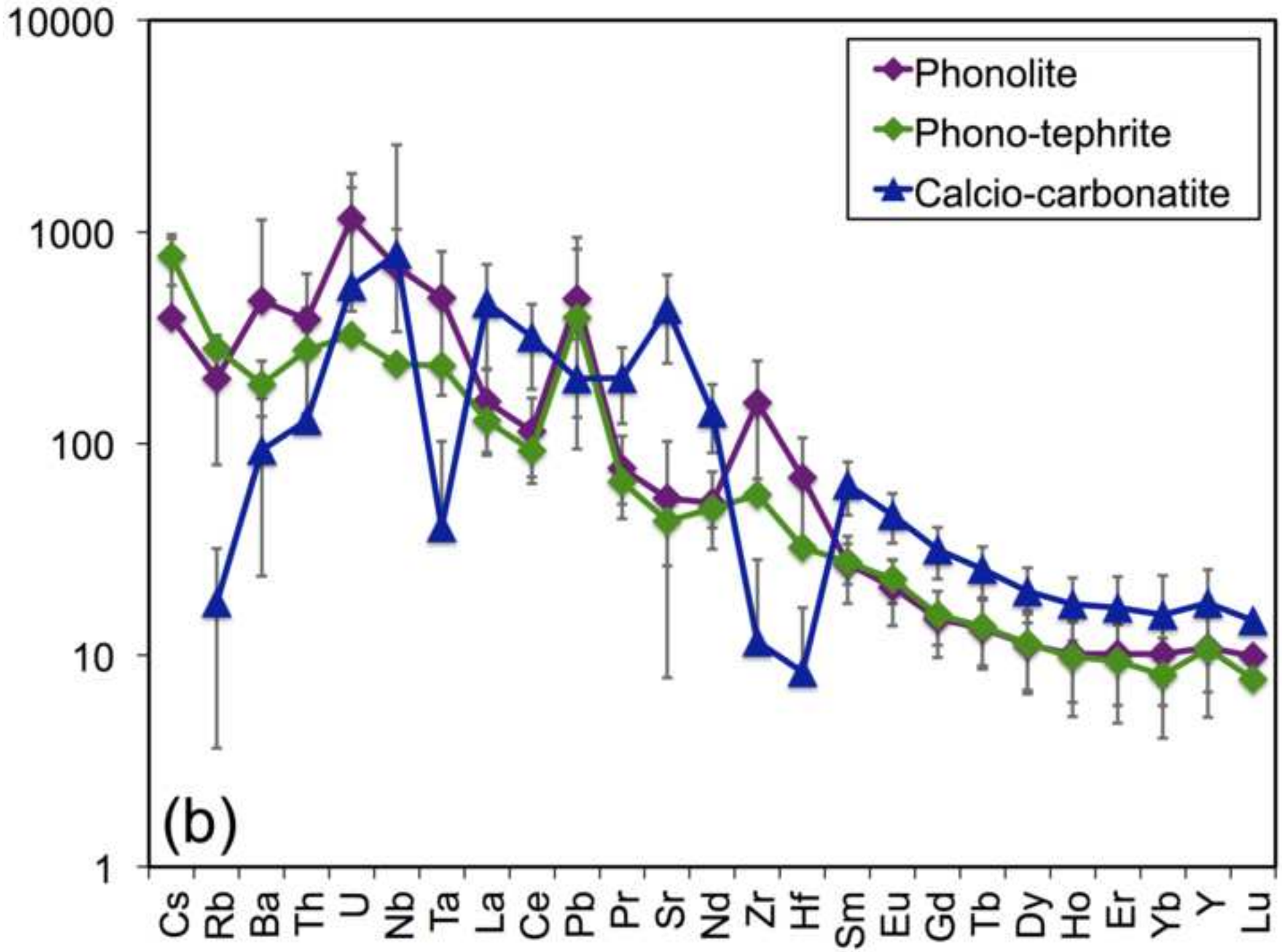

Bodeving, S., Williams-Jones, A.E., Swinden, S., 2017. Carbonate–silicate melt immiscibility, REE mineralising fluids, and the evolution of the Lofdal Intrusive Suite, Namibia. Lithos 268–271, 383-398. http://dx.doi.org/10.1016/j.lithos.2016.11.024.

Figure 3c

Click here to download high resolution image

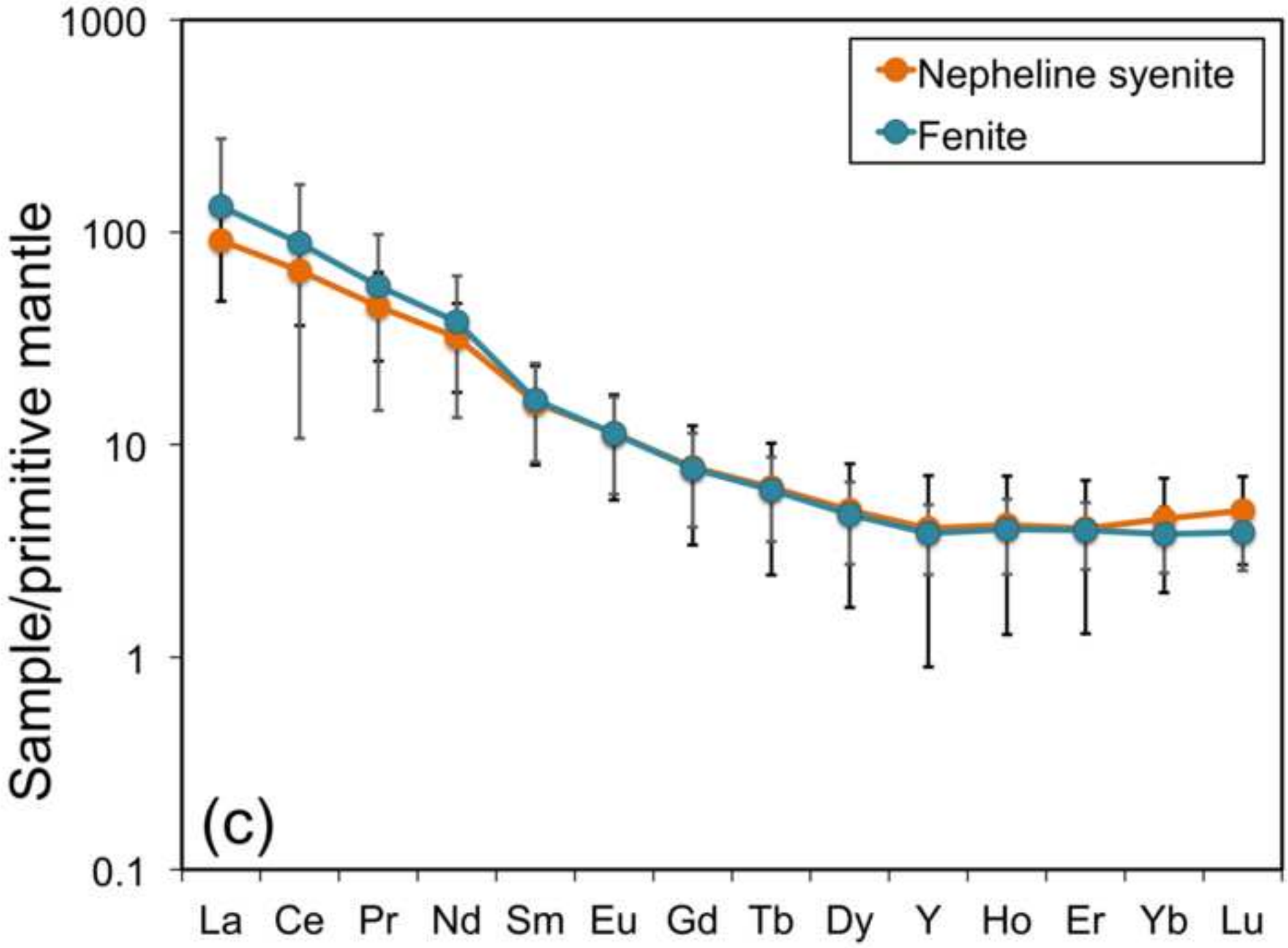

Bodeving, S., Williams-Jones, A.E., Swinden, S., 2017. Carbonate–silicate melt immiscibility, REE mineralising fluids, and the evolution of the Lofdal Intrusive Suite, Namibia. Lithos 268–271, 383-398. http://dx.doi.org/10.1016/j.lithos.2016.11.024.

Figure 3d

Click here to download high resolution image

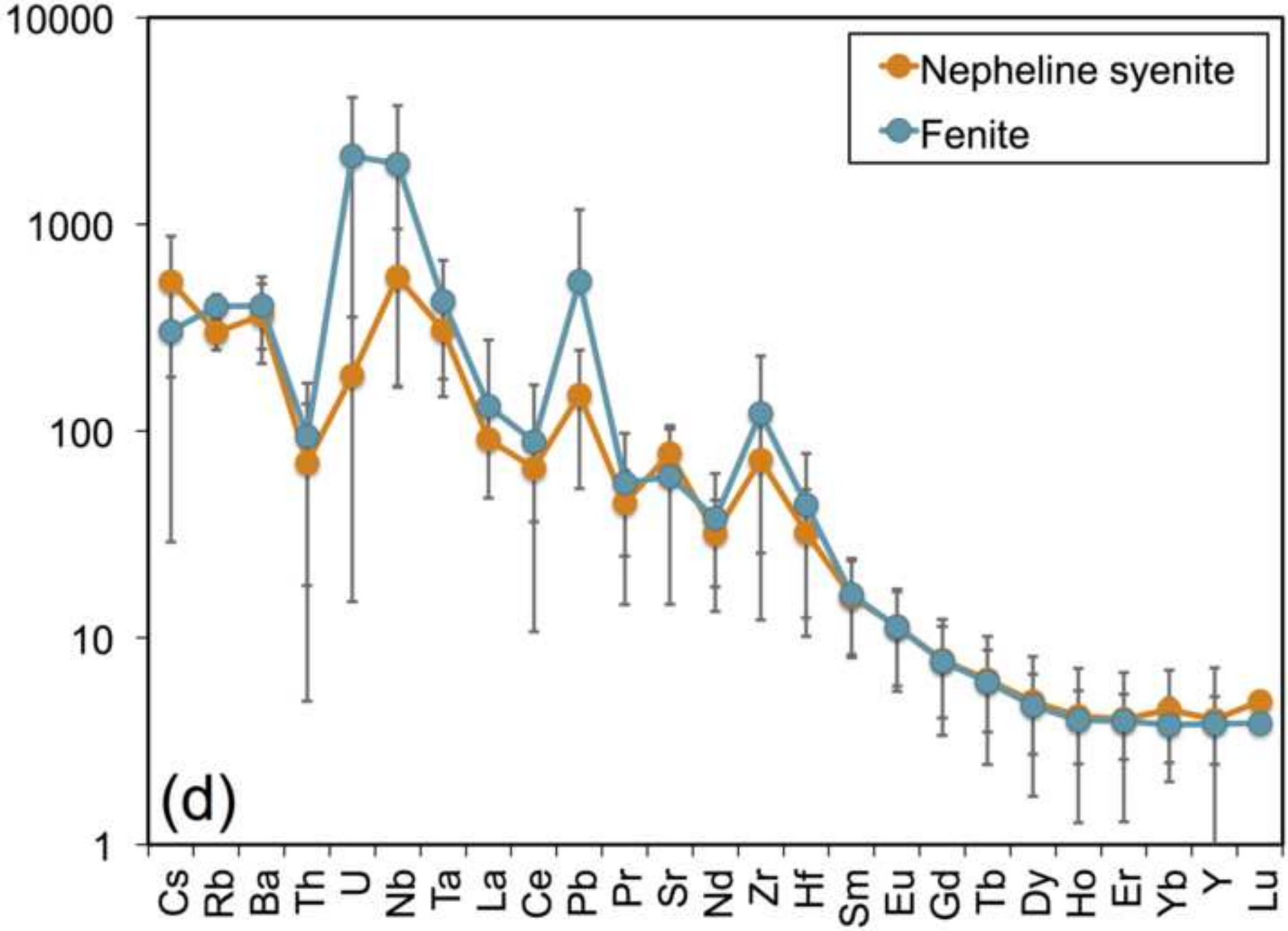

Bodeving, S., Williams-Jones, A.E., Swinden, S., 2017. Carbonate–silicate melt immiscibility, REE mineralising fluids, and the evolution of the Lofdal Intrusive Suite, Namibia. Lithos 268–271, 383-398. http://dx.doi.org/10.1016/j.lithos.2016.11.024.

Figure 4

Click here to download high resolution image

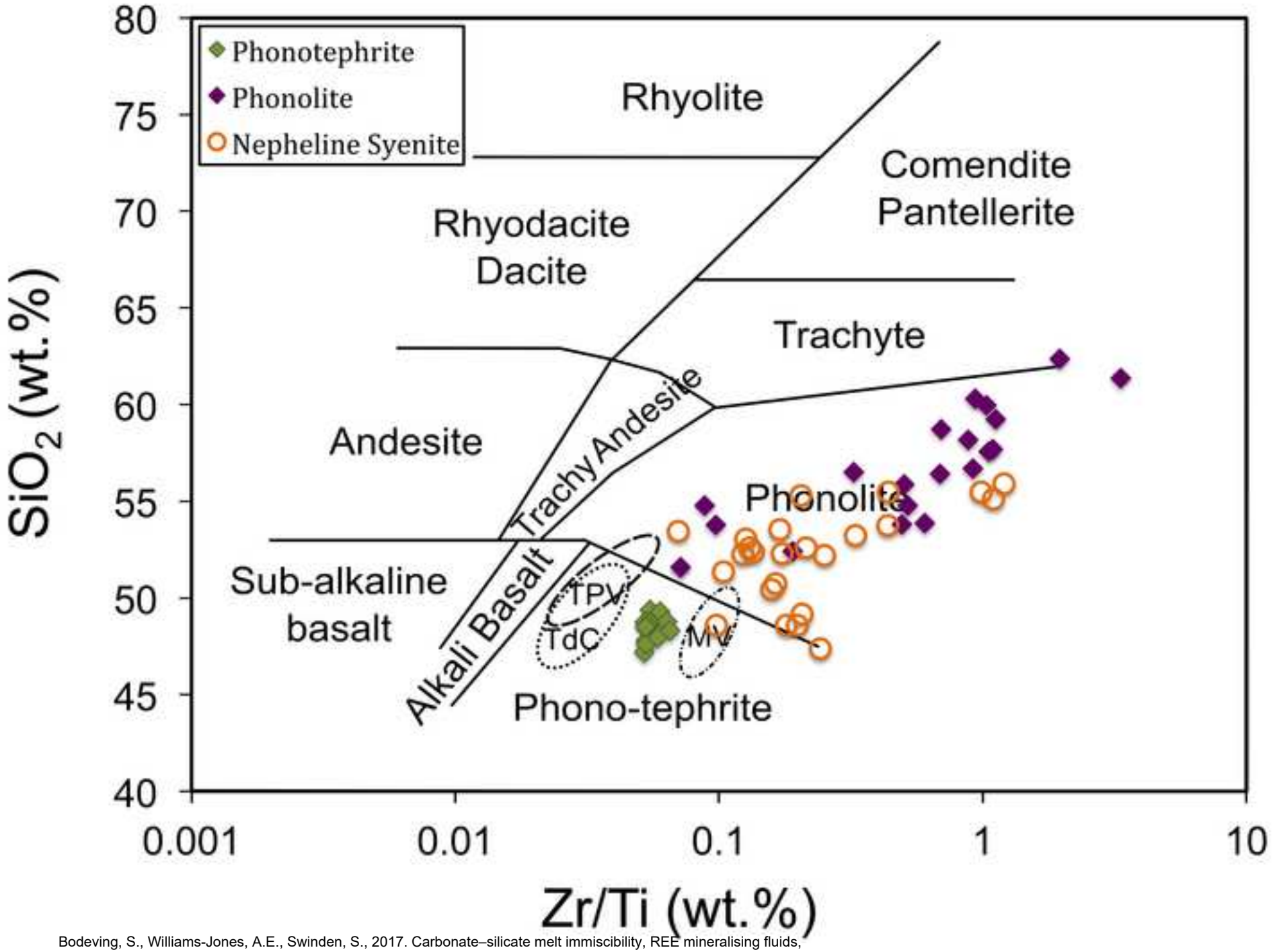

Bodeving, S., Williams-Jones, A.E., Swinden, S., 2017. Carbonate–silicate melt immiscibility, REE mineralising fluids, and the evolution of the Lofdal Intrusive Suite, Namibia. Lithos 268–271, 383-398. http://dx.doi.org/10.1016/j.lithos.2016.11.024.

Figure 5

Click here to download high resolution image

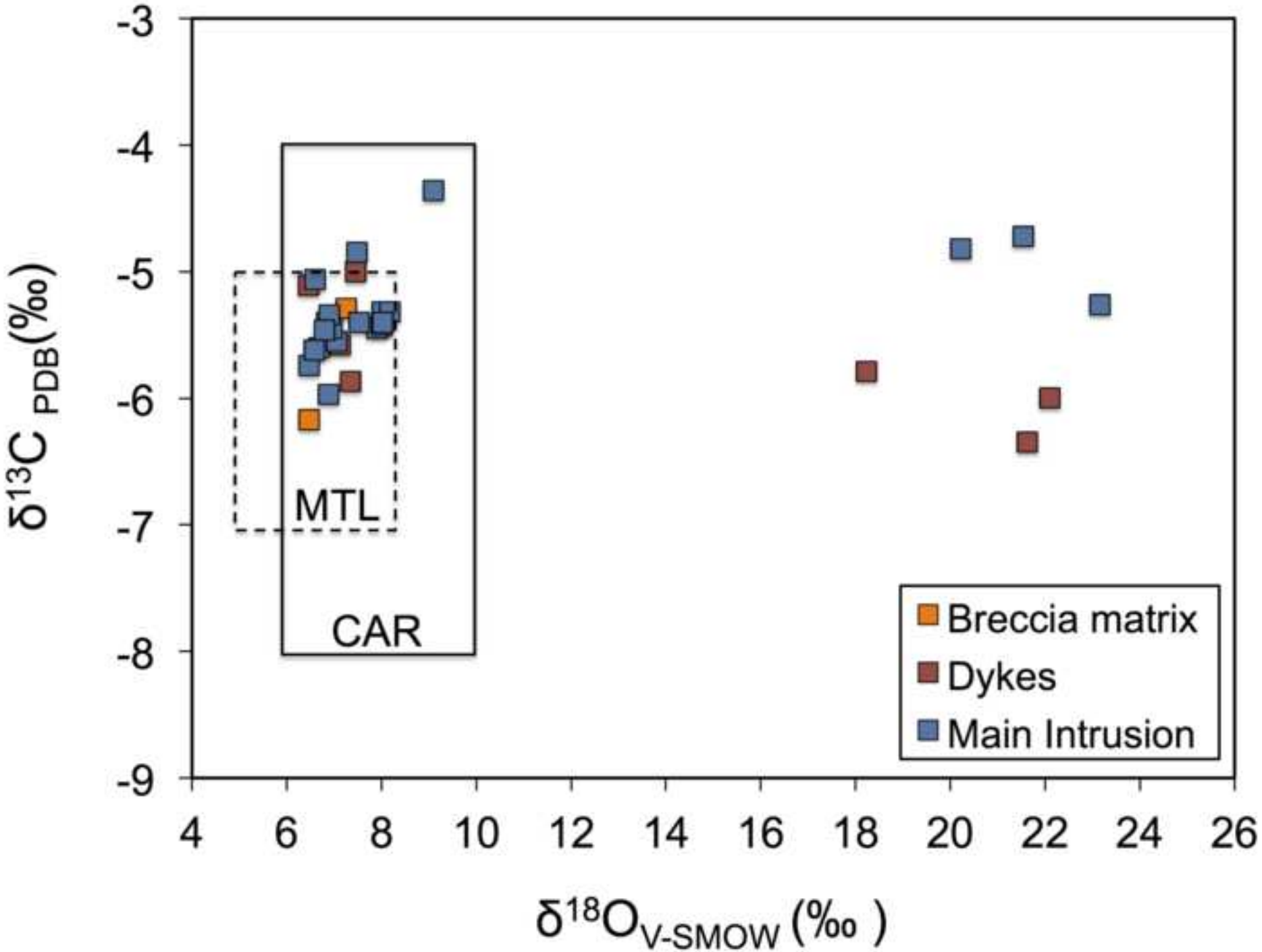

Bodeving, S., Williams-Jones, A.E., Swinden, S., 2017. Carbonate–silicate melt immiscibility, REE mineralising fluids, and the evolution of the Lofdal Intrusive Suite, Namibia. Lithos 268–271, 383-398. http://dx.doi.org/10.1016/j.lithos.2016.11.024.

Figure 6a

Click here to download high resolution image

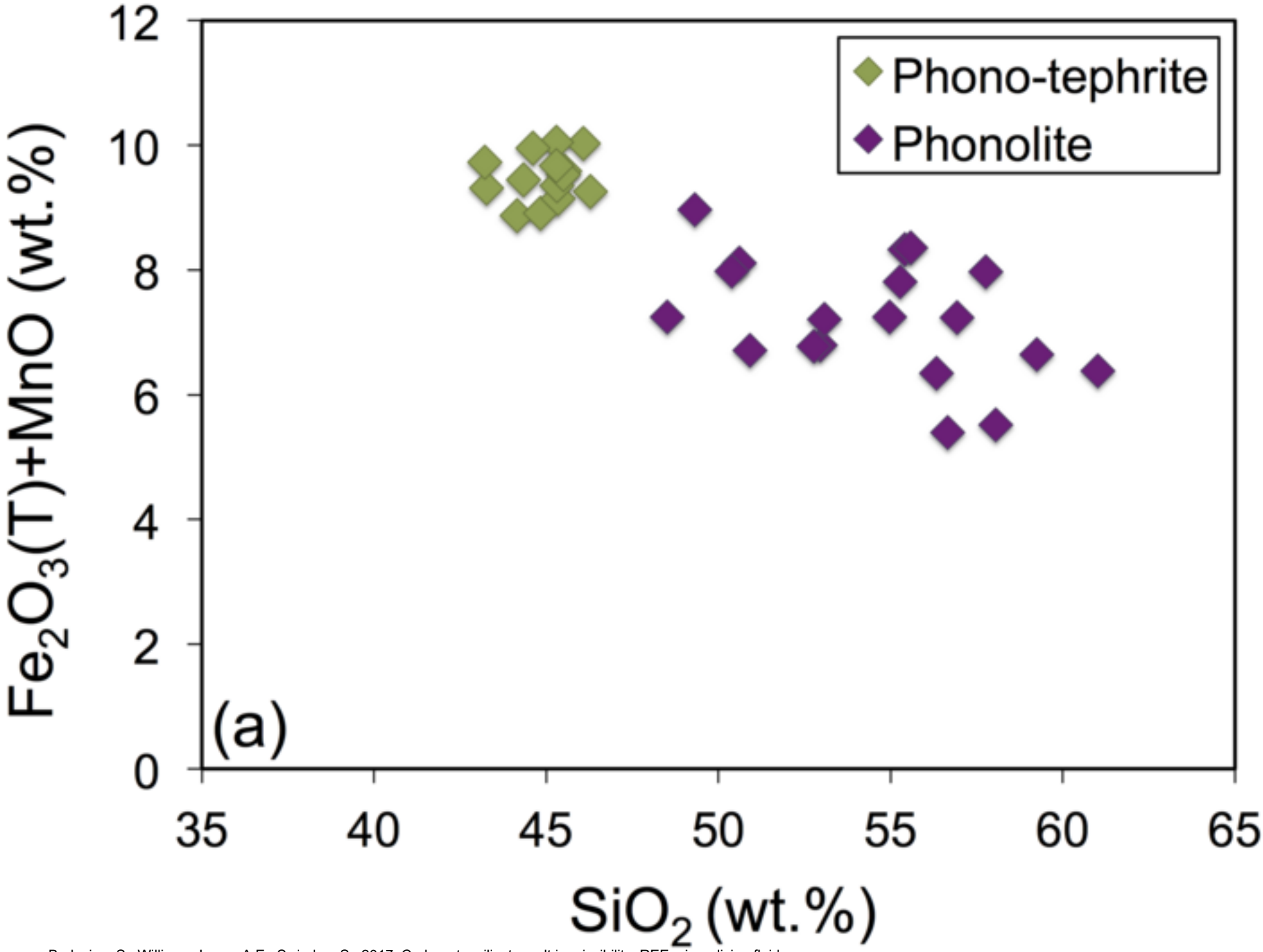

Bodeving, S., Williams-Jones, A.E., Swinden, S., 2017. Carbonate–silicate melt immiscibility, REE mineralising fluids, and the evolution of the Lofdal Intrusive Suite, Namibia. Lithos 268–271, 383-398. http://dx.doi.org/10.1016/j.lithos.2016.11.024.

Figure 6b

Click here to download high resolution image

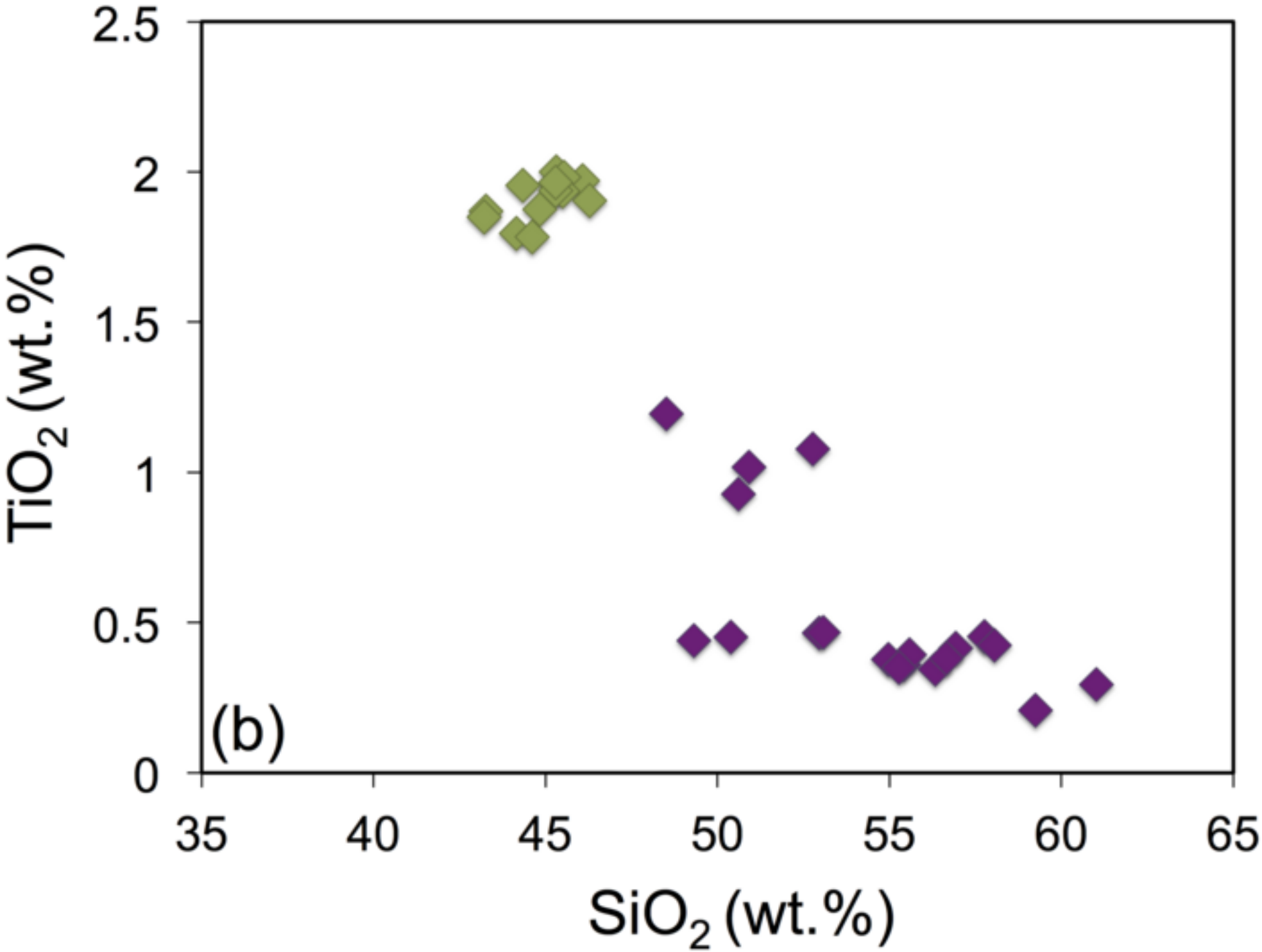

Bodeving, S., Williams-Jones, A.E., Swinden, S., 2017. Carbonate–silicate melt immiscibility, REE mineralising fluids, and the evolution of the Lofdal Intrusive Suite, Namibia. Lithos 268–271, 383-398. http://dx.doi.org/10.1016/j.lithos.2016.11.024.

Figure 6c

Click here to download high resolution image

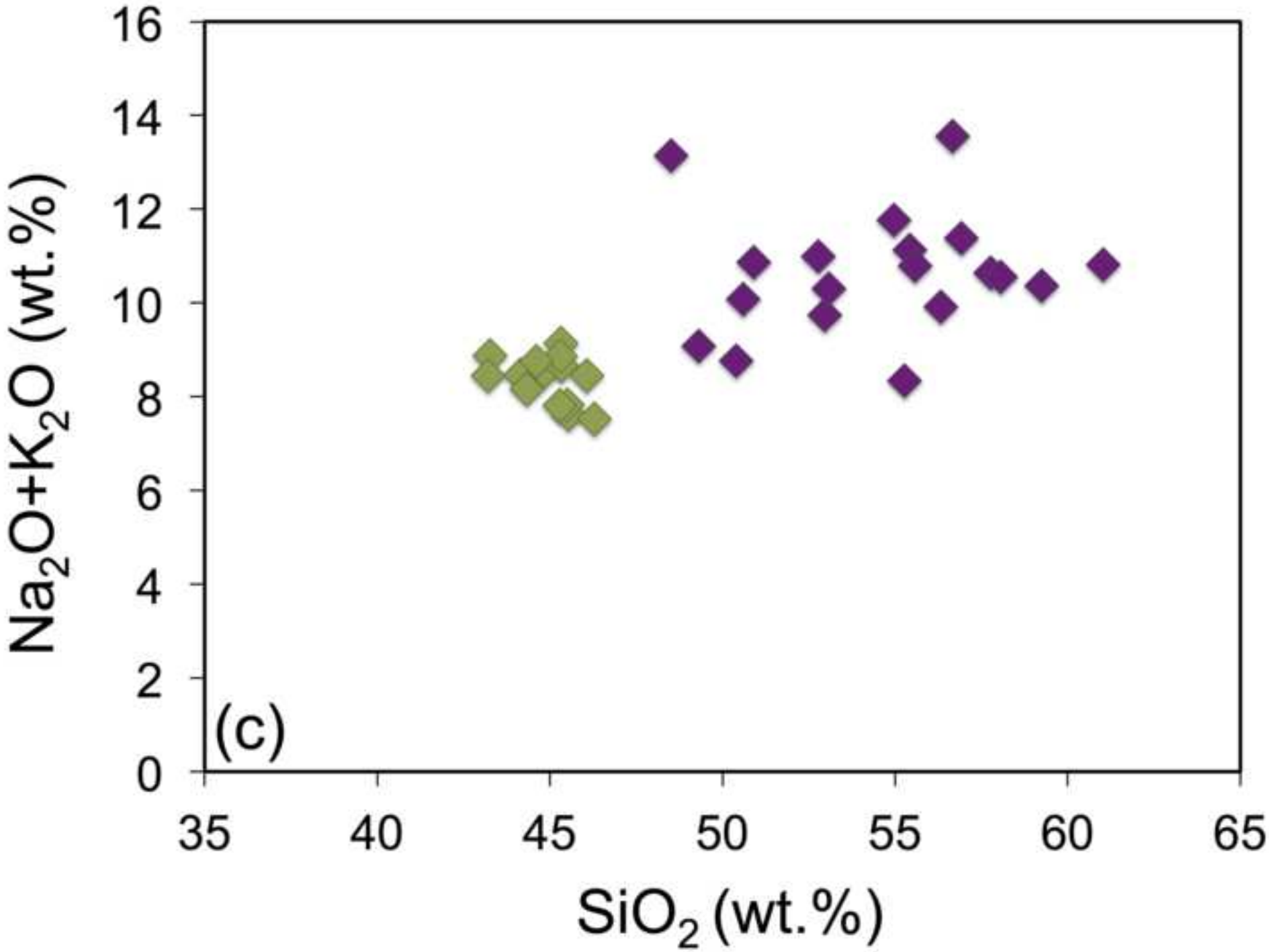

Bodeving, S., Williams-Jones, A.E., Swinden, S., 2017. Carbonate–silicate melt immiscibility, REE mineralising fluids, and the evolution of the Lofdal Intrusive Suite, Namibia. Lithos 268–271, 383-398. http://dx.doi.org/10.1016/j.lithos.2016.11.024.

Figure 6d

Click here to download high resolution image

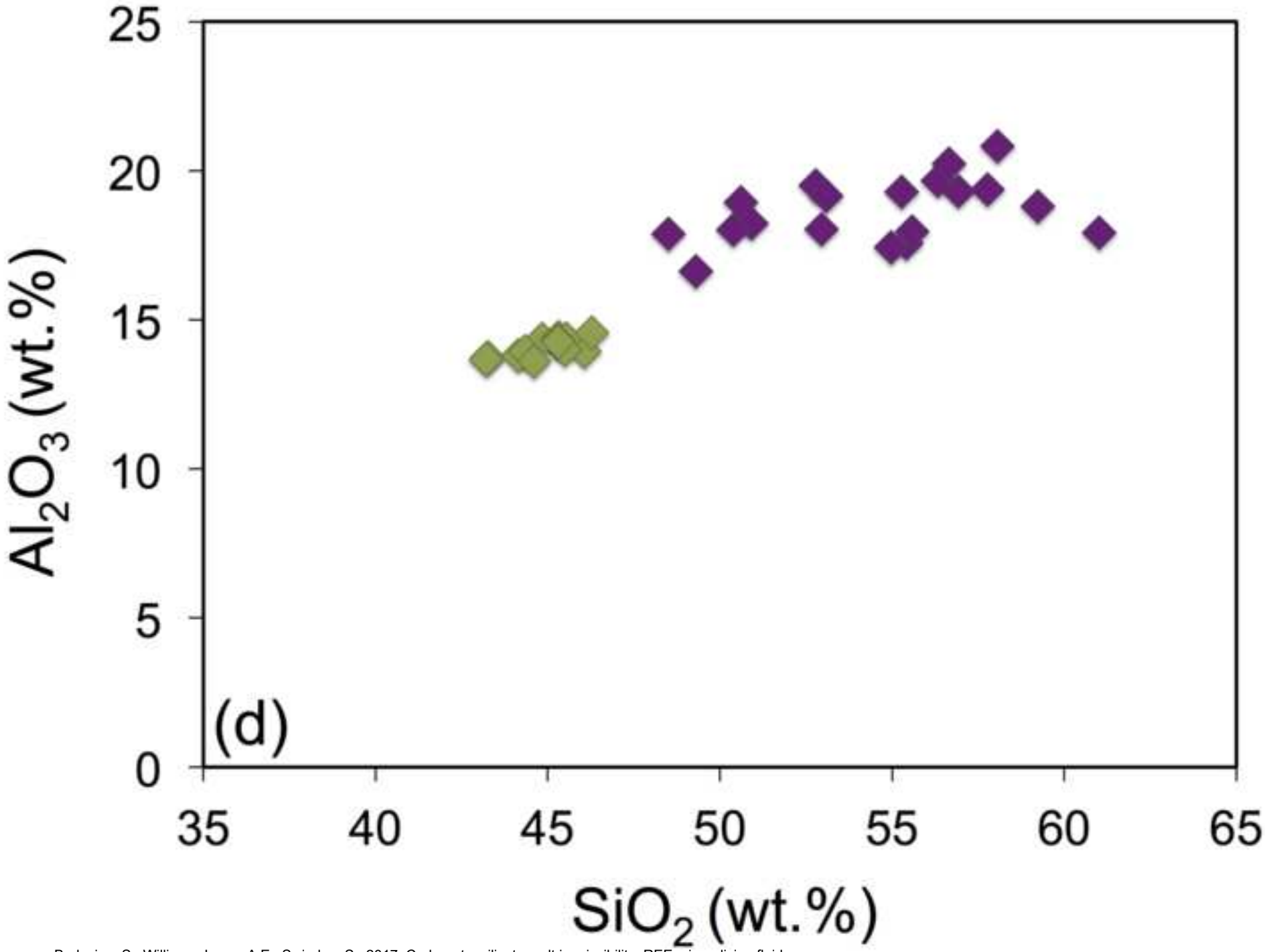

Bodeving, S., Williams-Jones, A.E., Swinden, S., 2017. Carbonate–silicate melt immiscibility, REE mineralising fluids, and the evolution of the Lofdal Intrusive Suite, Namibia. Lithos 268–271, 383-398. http://dx.doi.org/10.1016/j.lithos.2016.11.024.

Figure 7a

Click here to download high resolution image

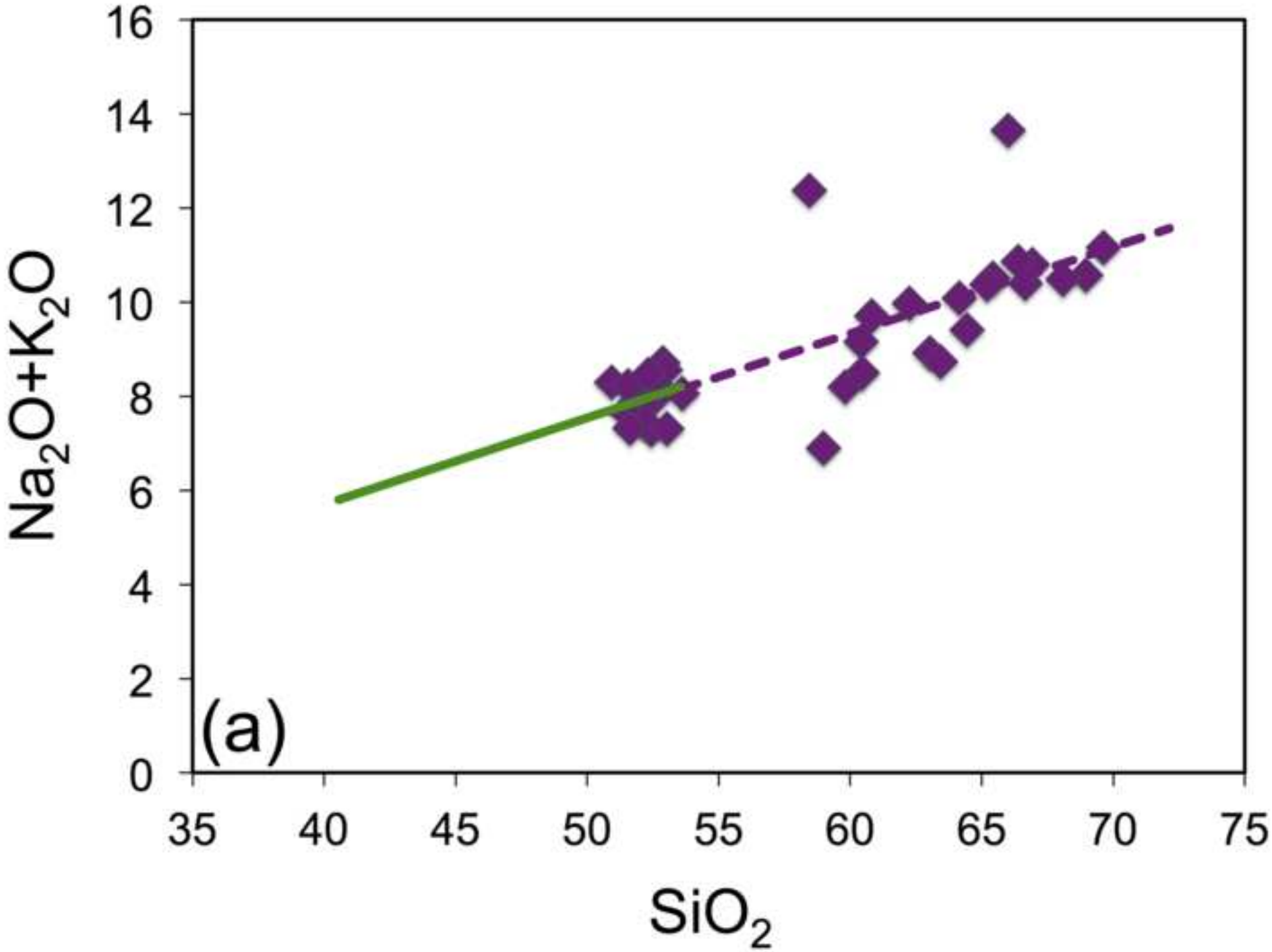

Bodeving, S., Williams-Jones, A.E., Swinden, S., 2017. Carbonate–silicate melt immiscibility, REE mineralising fluids, and the evolution of the Lofdal Intrusive Suite, Namibia. Lithos 268–271, 383-398. http://dx.doi.org/10.1016/j.lithos.2016.11.024.

Figure 7b

Click here to download high resolution image

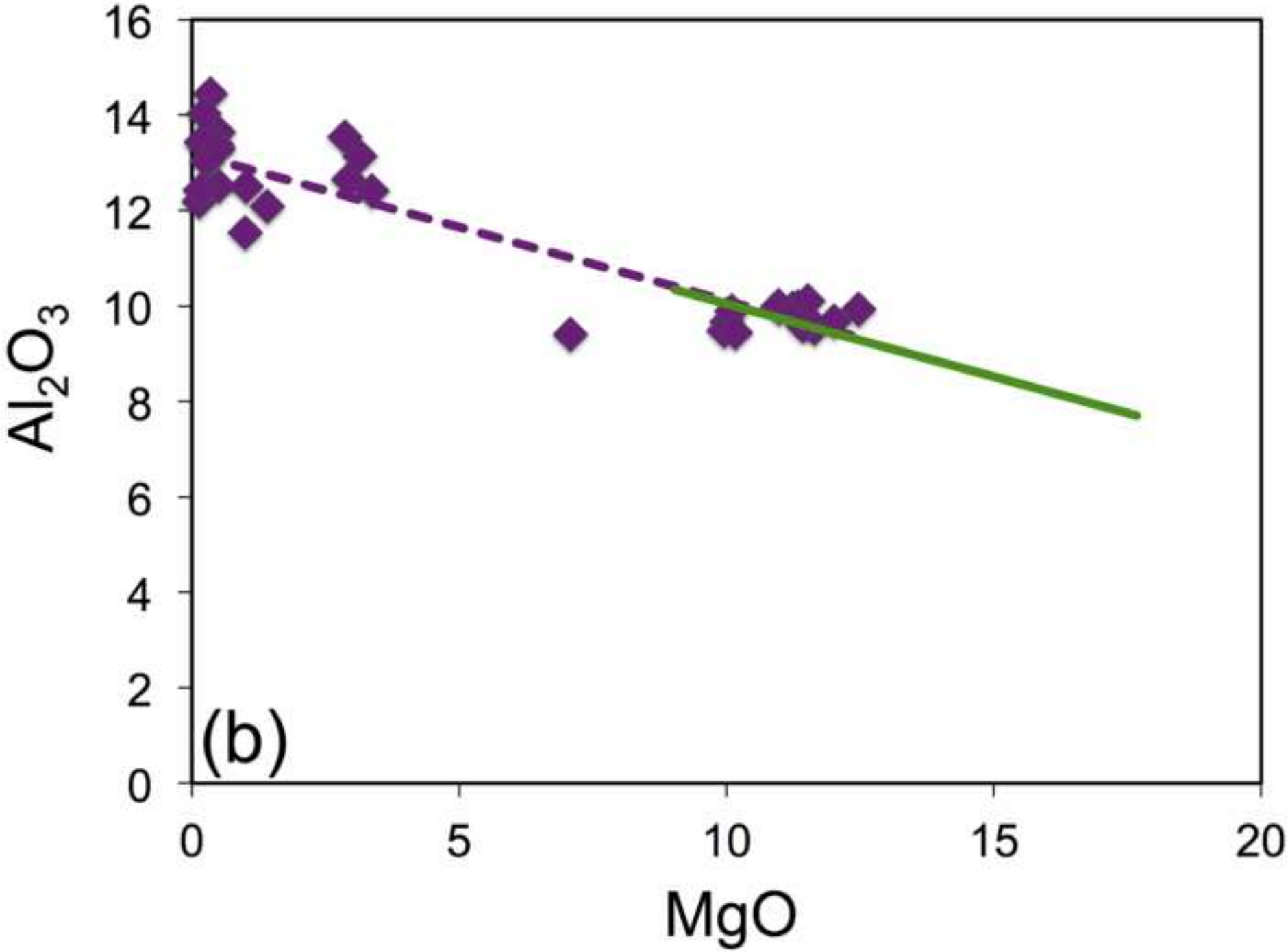

Bodeving, S., Williams-Jones, A.E., Swinden, S., 2017. Carbonate–silicate melt immiscibility, REE mineralising fluids, and the evolution of the Lofdal Intrusive Suite, Namibia. Lithos 268–271, 383-398. http://dx.doi.org/10.1016/j.lithos.2016.11.024.

Figure 7c

Click here to download high resolution image

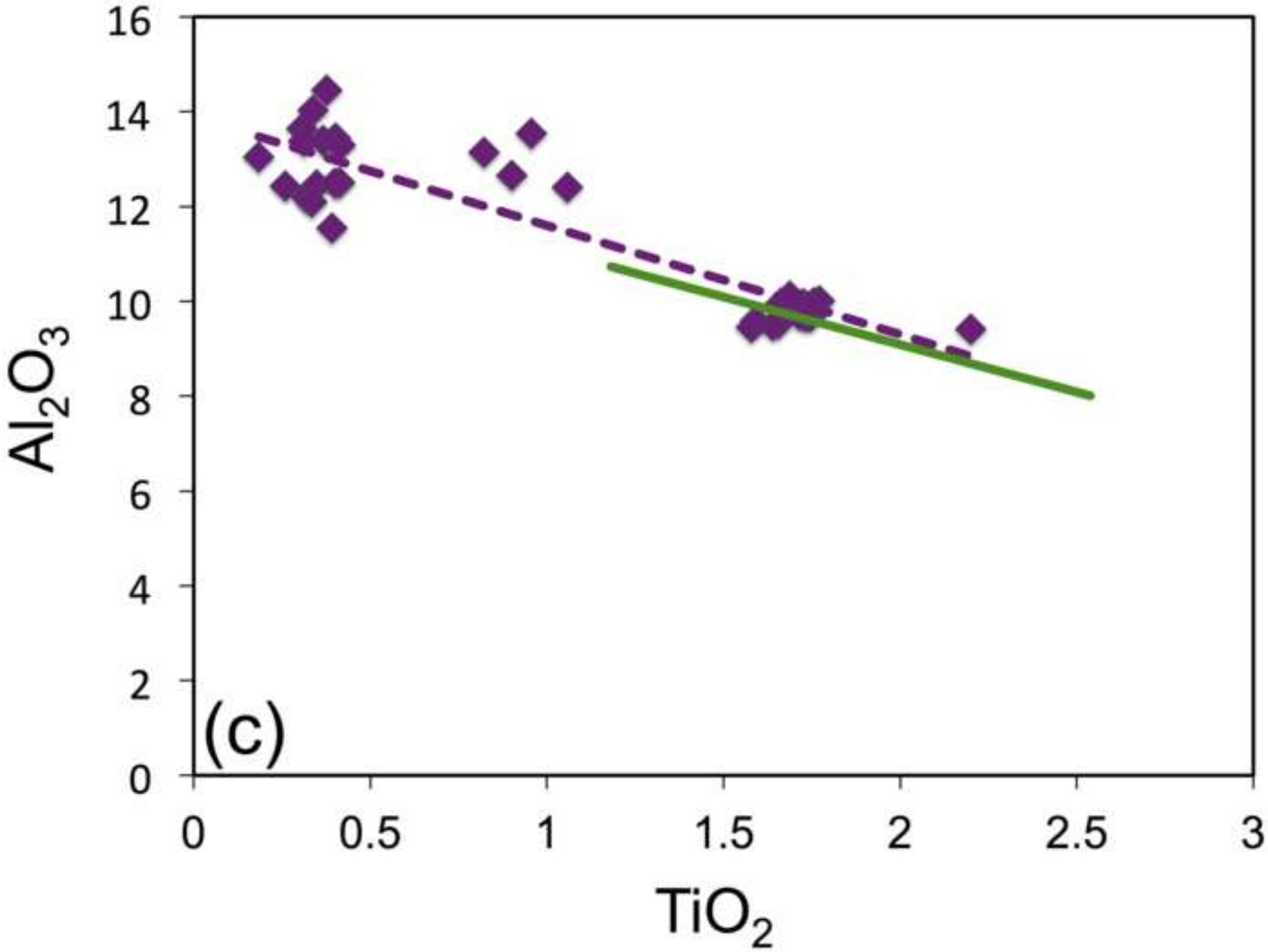

Bodeving, S., Williams-Jones, A.E., Swinden, S., 2017. Carbonate–silicate melt immiscibility, REE mineralising fluids, and the evolution of the Lofdal Intrusive Suite, Namibia. Lithos 268–271, 383-398. http://dx.doi.org/10.1016/j.lithos.2016.11.024.

Figure 7d

Click here to download high resolution image

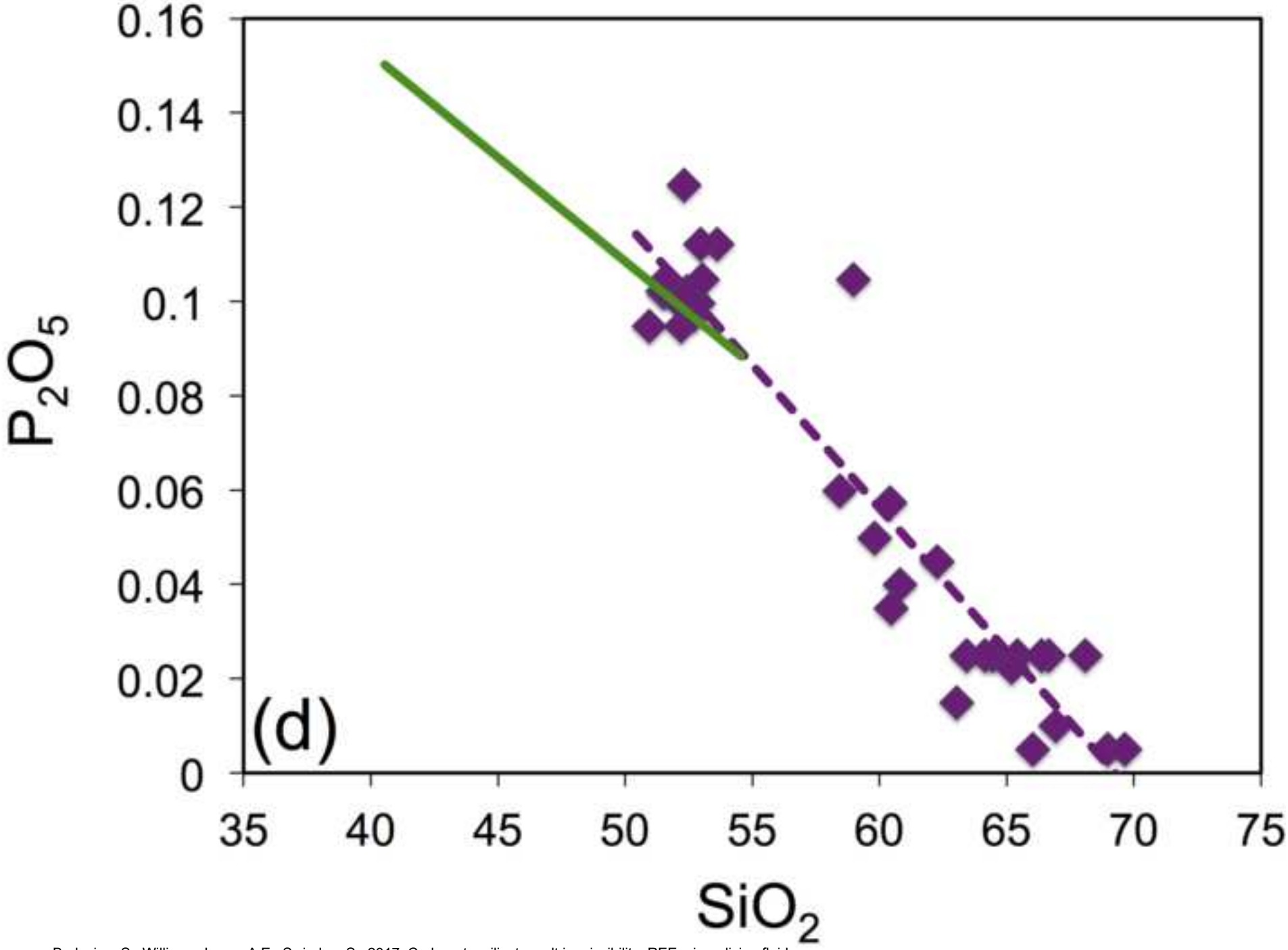

Bodeving, S., Williams-Jones, A.E., Swinden, S., 2017. Carbonate–silicate melt immiscibility, REE mineralising fluids, and the evolution of the Lofdal Intrusive Suite, Namibia. Lithos 268–271, 383-398. http://dx.doi.org/10.1016/j.lithos.2016.11.024.

Figure 8

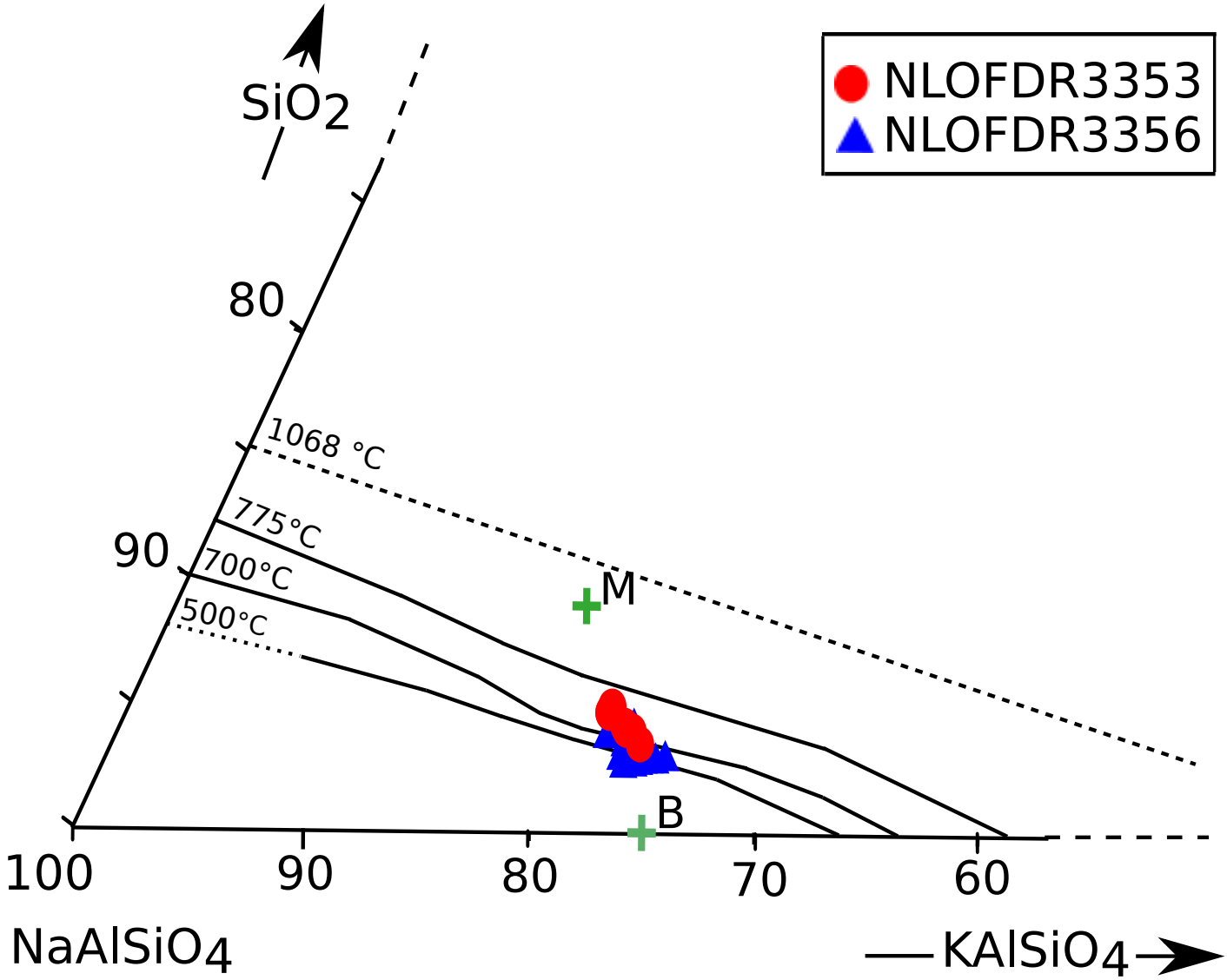

Bodeving, S., Williams-Jones, A.E., Swinden, S., 2017. Carbonate–silicate melt immiscibility, REE mineralising fluids, and the evolution of the Lofdal Intrusive Suite, Namibia. Lithos 268–271, 383-398. http://dx.doi.org/10.1016/j.lithos.2016.11.024.

Figure 9a

Click here to download high resolution image

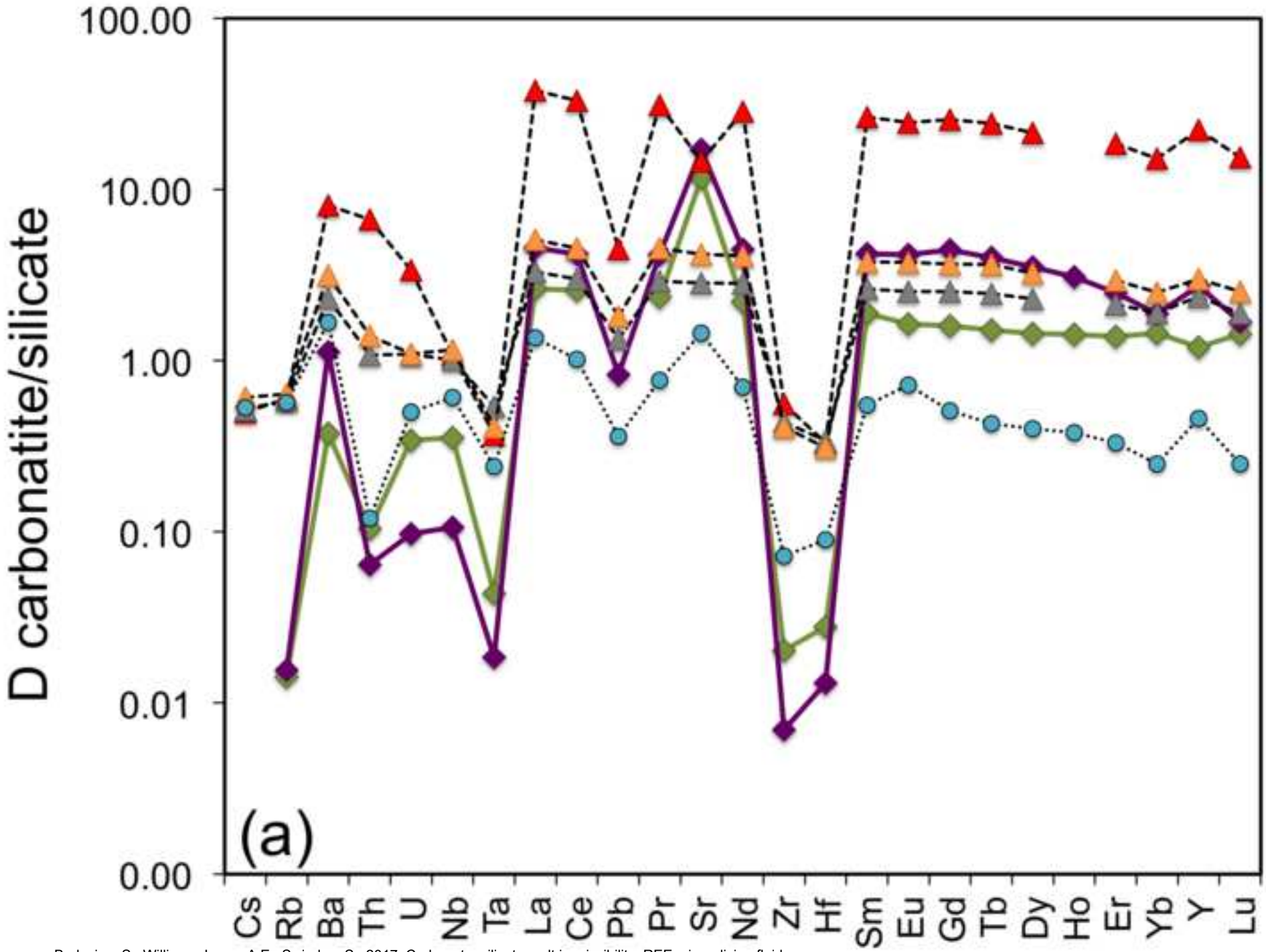

Bodeving, S., Williams-Jones, A.E., Swinden, S., 2017. Carbonate–silicate melt immiscibility, REE mineralising fluids, and the evolution of the Lofdal Intrusive Suite, Namibia. Lithos 268–271, 383-398. http://dx.doi.org/10.1016/j.lithos.2016.11.024.

Figure 9b

Click here to download high resolution image

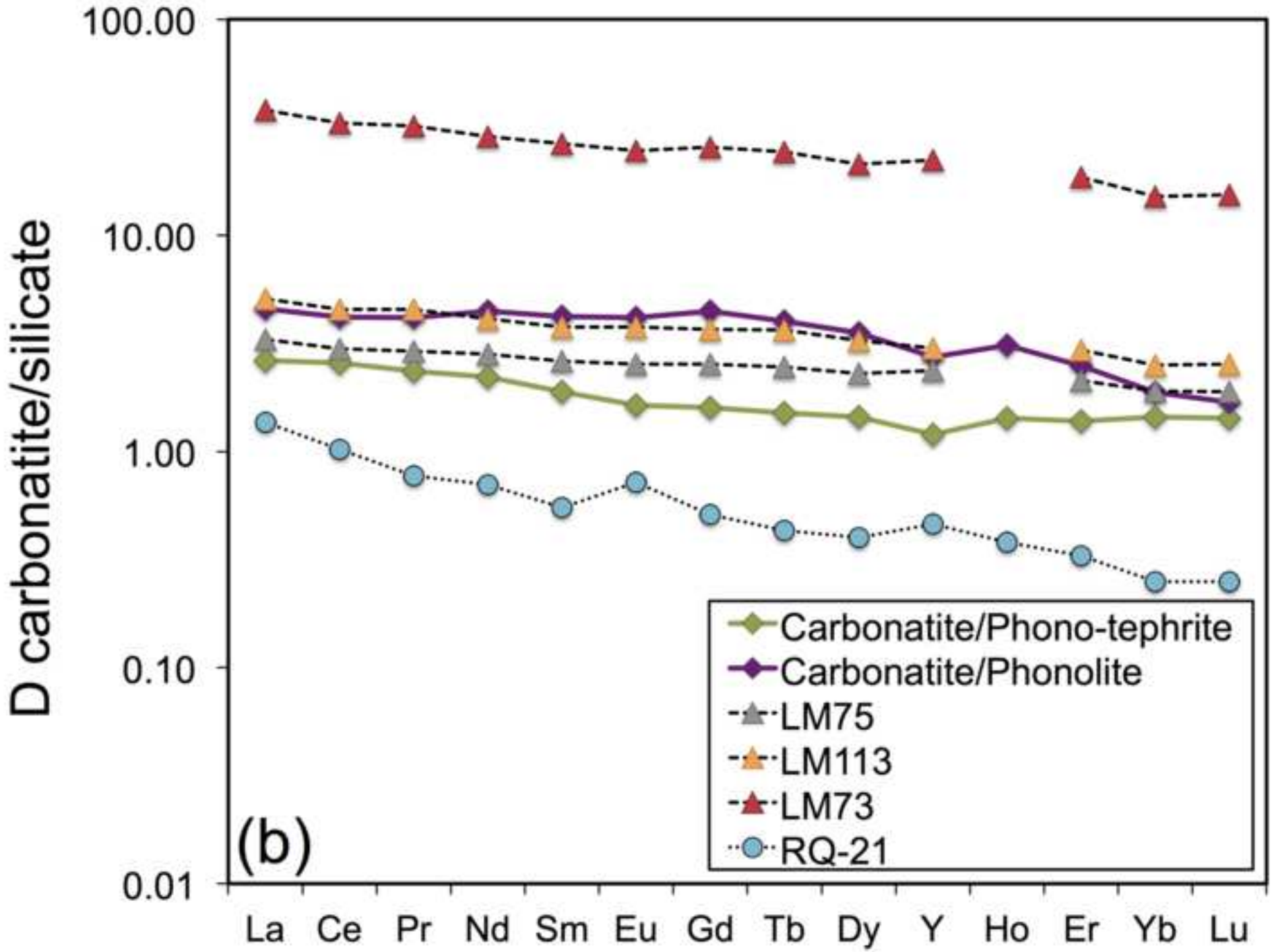

Bodeving, S., Williams-Jones, A.E., Swinden, S., 2017. Carbonate–silicate melt immiscibility, REE mineralising fluids, and the evolution of the Lofdal Intrusive Suite, Namibia. Lithos 268–271, 383-398. http://dx.doi.org/10.1016/j.lithos.2016.11.024.

Figure 10

Click here to download high resolution image

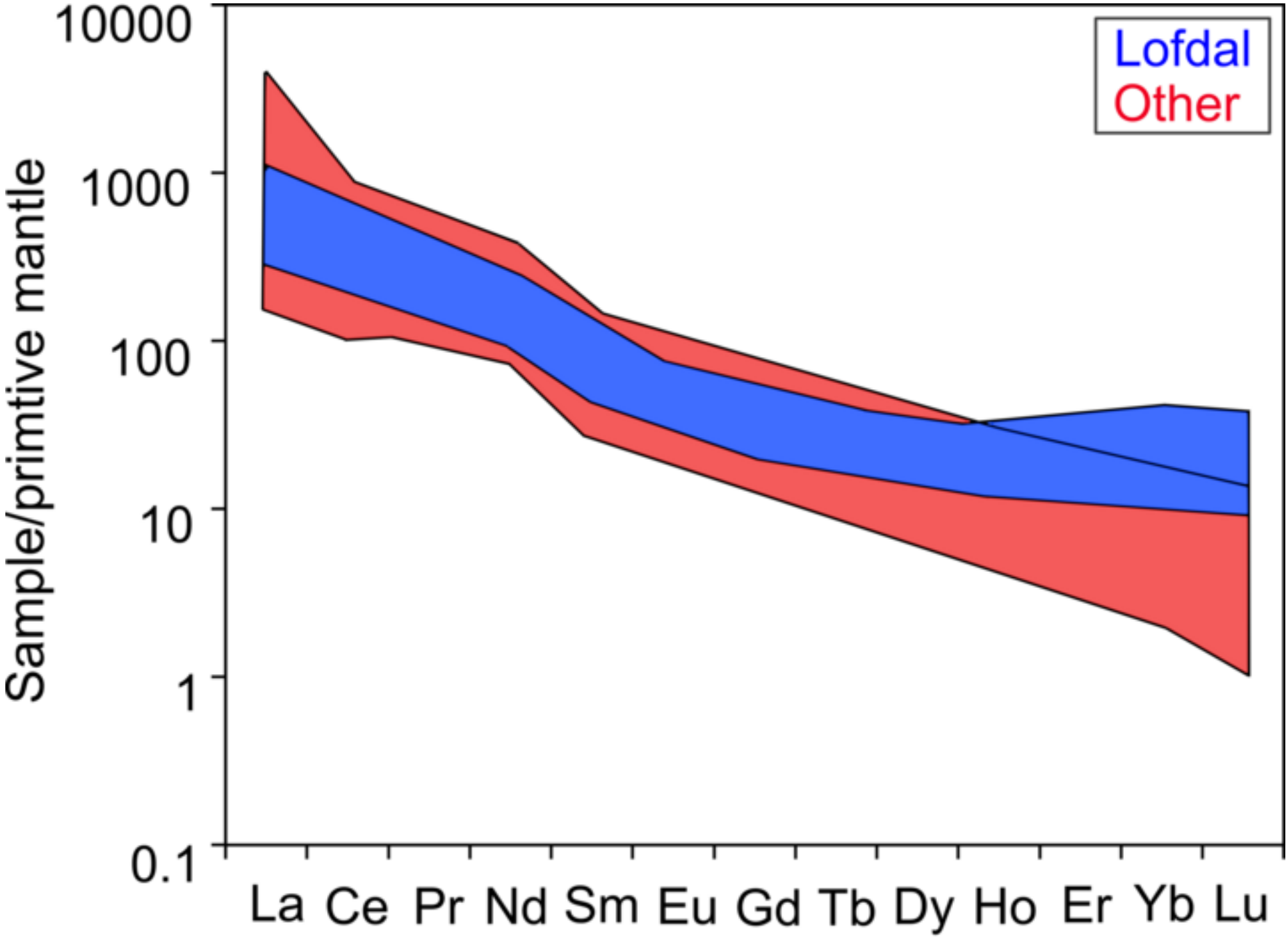

Bodeving, S., Williams-Jones, A.E., Swinden, S., 2017. Carbonate–silicate melt immiscibility, REE mineralising fluids, and the evolution of the Lofdal Intrusive Suite, Namibia. Lithos 268–271, 383-398. http://dx.doi.org/10.1016/j.lithos.2016.11.024.

Table

Click here to download Table: Tables.docx

Bodeving, S., Williams-Jones, A.E., Swinden, S., 2017. Carbonate–silicate melt immiscibility, REE mineralising fluids, and the evolution of the Lofdal Intrusive Suite, Namibia. Lithos 268–271, 383-398. http://dx.doi.org/10.1016/j.lithos.2016.11.024.

Table 1: Average compositions of the different members of the Lofdal Intrusive Suite

Rock Type	Carbonatite	Nepheline Syenite	Phonolite	Phono-tephrite	Fenite
Sample #	n=16	n=24	n=19	n=14	n=19
wt.%					
SiO_2	3.92±0.87	49.31±0.56	54.48±0.76	44.93±0.25	54.39±1.05
Al_2O_3	0.70±0.17	19.66±0.33	18.41±0.34	14.10±0.08	16.64±0.30
Fe_2O_3	3.60±0.71	5.53±0.23	7.23±0.31	9.27±0.10	2.60±0.50
MnO	0.77±0.12	0.20±0.01	0.22±0.02	0.22±0.01	0.18±0.02
MgO	0.19±0.04	0.45±0.09	0.76±0.22	6.32±0.12	0.13±0.03
CaO	47.83±1.00	4.55±0.31	3.76±0.47	7.25±0.14	6.20±0.60
Na_2O	0.40±0.19	7.32±0.30	5.63±0.42	4.27±0.10	2.48±0.24
K_2O	0.30±0.08	6.48±0.21	4.80±0.50	4.10±0.11	10.11±0.50
TiO_2	0.05±0.02	0.57±0.05	0.63±0.12	1.91±0.02	0.21±0.06
P_2O_5	0.74±0.33	0.32±0.07	0.13±0.02	0.42±0.01	0.51±0.11
LOI	38.53±1.11	4.77±0.33	3.11±0.32	6.49±0.26	5.55±0.50
Total	97.03±0.32	99.16±0.19	99.16±0.24	99.28±0.22	99.01±0.26
ppm					
Sc	5.13±1.12	2.50±0.49	7.00±2.09	16.57±0.33	<1
Be	1.00±0.00	3.17±0.42	5.70±0.70	4.29±0.16	2.29±0.11
V	30.79±11.28	46.83±4.39	44.00±14.82	163.71±2.31	23.00±6.65
Cr	40.00±40.00	55.00±4.33	66.00±6.04	466.43±17.24	<20
Co	4.50±0.69	3.08±0.47	5.72±1.50	31.07±1.09	2.63±0.46
Ni	<20	<20	35.00±1.58	134.29±4.02	<20
Cu	20.91±5.86	16.67±1.18	26.7±3.92	25.83±3.69	76.00±30.03
Zn	74.17±13.88	107.27±5.24	192.22±35.79	148.57±10.21	173.08±43.13
Ga	6.31±0.91	27.75±0.65	39.15±2.80	23.64±0.20	35.35±3.18
Ge	1.33±0.14	1.23±0.09	2.00±0.07	2.00±0.00	1.50±0.12
As	8.25±0.80	<5	11.57±1.98	10.91±1.20	5.50±0.16
Rb	11.29±2.24	190.83±7.12	128.35±17.42	178.64±3.73	253.80±8.45
Sr	9121.19±1017.20	1644.83±102.92	1165.50±223.69	908.71±93.89	1272.15±221.60
Y	80.13±8.73	18.33±2.91	49.55±4.29	48.71±6.85	17.40±1.44
Zr	129.63±46.99	813.79±107.49	1752.10±221.40	641.50±12.55	1362.60±281.26
Nb	561.93±317.89	395.63±57.10	487.11±55.18	168.93±4.11	1392.95±292.65
Mo	11.88±2.31	<2	4±0.35	5.00±0.69	8.67±2.26
Ag	2.01±0.32	3.96±0.36	3.85±0.18	4.68±0.21	3.80±0.40
Sn	5.00±1.21	2.00±0.14	4.89±0.57	3.21±0.11	1.75±0.20
Sb	1.50±0.39	0.73±0.05	0.74±0.04	0.73±0.03	0.71±0.04
Cs	<0.5	4.18±0.56	3.12±0.94	6.05±0.44	2.40±0.50
Ba	652.56±121.82	2531.00±215.44	3305.45±1043.36	1328.29±104.55	2817.05±247.54
Bi	0.67±0.04	<0.4	<0.4	0.90±0.08	<0.4
La	316.94±41.04	62.85±6.19	108.68±10.36	87.75±7.33	90.72±22.68

Bodeving, S., Williams-Jones, A.E., Swinden, S., 2017. Carbonate–silicate melt immiscibility, REE mineralising fluids, and the evolution of the Lofdal Intrusive Suite, Namibia. Lithos 268–271, 383-398. http://dx.doi.org/10.1016/j.lithos.2016.11.024.

Table 1 continued:

Rock Type	Carbonatite	Nepheline Syenite	Phonolite	Phono-tephrite	Fenite
Sample #	n=16	n=24	n=19	n=14	n=19
Ce	565.13±61.31	117.10±10.72	202.79±19.64	164.64±11.02	158.14±31.92
Pr	56.35±5.54	12.34±1.12	21.05±1.98	18.19±1.04	15.46.±2.63
Nd	189.81±16.83	43.27±3.96	71.22±6.34	66.56±3.33	51.28±7.60
Sm	28.43±2.01	7.00±0.70	12.01±0.94	12.24±0.71	7.21±0.81
Eu	7.73±0.51	1.91±0.20	3.51±0.27	3.85±0.24	1.90±0.21
Gd	18.77±1.28	4.66±0.54	8.87±0.69	9.28±0.71	4.60±0.49
Tb	2.76±0.19	0.68±0.08	1.45±0.12	1.48±0.14	0.66±0.06
Dy	14.76±1.08	3.63±0.48	8.25±0.72	8.40±0.95	3.47±0.33
Ho	2.86±0.24	0.69±0.10	1.67±0.15	1.61±0.20	0.66±0.06
Er	8.04±0.82	1.94±0.27	4.86±0.46	4.50±0.59	1.90±0.15
Tm	1.20±0.14	0.32±0.04	0.76±0.08	0.64±0.08	0.29±0.02
Yb	7.64±1.03	2.21±0.25	4.99±0.48	3.97±0.53	1.87±0.15
Lu	1.08±0.15	0.36±0.03	0.73±0.06	0.57±0.07	0.29±0.02
Hf	2.56±0.66	10.00±1.25	21.32±2.59	9.98±0.10	13.62±2.41
Ta	1.65±0.64	12.60±1.35	20.05±2.94	9.55±0.11	17.40±2.32
W	1.50±0.19	3.73±0.96	2.88±0.54	3.23±0.88	1.80±0.30
Tl	<0.1	0.25±0.02	0.31±0.04	0.44±0.08	0.18±0.02
Pb	14.40±1.93	10.59±1.40	34.21±5.54	27.85±10.42	37.68±10.52
Th	10.95±4.53	5.97±1.13	32.82±4.71	23.59±3.62	8.03±1.49
U	11.63±5.57	3.89±0.73	24.28±3.45	6.82±0.15	45.14±9.42
mg #		12.66	15.97	54.87	
PI		0.97	0.79	0.81	
Y/Ho	27.32±0.66	25.85±0.54	29.52±0.43	29.15±0.08	
Nb/Ta	352.30±64.22	31.33±2.09	30.53±2.34	17.67±0.31	
Zr/Hf	63.59±7.89	80.60±1.91	80.77±2.59	64.28±1.01	

*Note: mg # = 100*MgO/(MgO+FeO) (molar ratio); peralkalinity index PI = (Na_2O+K_2O)/Al_2O_3 (molar ratio);* #.## ± #.## represents the mean ± the mean of the standard deviation, $\sigma / n^{0.5}$, where σ is the standard deviation and n is the number of samples.

Bodeving, S., Williams-Jones, A.E., Swinden, S., 2017. Carbonate–silicate melt immiscibility, REE mineralising fluids, and the evolution of the Lofdal Intrusive Suite, Namibia. Lithos 268–271, 383-398. http://dx.doi.org/10.1016/j.lithos.2016.11.024.

Table 2: Oxygen and carbon isotope ratios for calcite in the carbonatite.

Sample	$\delta^{18}O_{V\text{-}SMOW}$ (‰)	$\delta^{13C}_{V\text{-}PDB}$ (‰)
18508	6.59	-5.06
MC2	6.68	-5.60
MC1	8.01	-5.32
3368	6.85	-5.40
3359	6.88	-5.97
3371	7.05	-5.55
18507	7.90	-5.45
3374	6.95	-5.45
SB-12-M13	6.47	-5.74
10298	8.00	-5.42
18765	8.17	-5.32
10304	7.48	-4.85
10298	8.00	-5.42
18504	7.53	-5.40
3379-1	21.54	-4.72
3378	20.22	-4.82
3379-2	6.58	-5.62
18518	23.16	-5.26
18597	6.90	-5.34
18596	6.79	-5.46
18706	8.02	-5.40
18558-1	6.46	-5.11
10314	22.10	-6.00
10313	21.63	-6.35
10355	7.46	-5.00
10464	7.34	-5.87
18574	6.84	-5.51
10280	7.13	-5.58
10284	18.24	-5.79
19210	6.48	-6.17
10341	7.25	-5.29

Note: σ=0.03‰

Bodeving, S., Williams-Jones, A.E., Swinden, S., 2017. Carbonate–silicate melt immiscibility, REE mineralising fluids, and the evolution of the Lofdal Intrusive Suite, Namibia. Lithos 268–271, 383-398. http://dx.doi.org/10.1016/j.lithos.2016.11.024.

Table 3: Fractional Crystallisation Model

	SiO_2	Al_2O_3	FeO	MnO	MgO	CaO	Na_2O	K_2O	TiO_2	P_2O_5	Total
Initial bulk melt	44.93	14.10	9.27	0.22	6.32	7.25	4.27	4.10	1.91	0.42	99.28
K-feldspar	64.50	18.30	0.17			0.06	0.46	15.75			99.24
Olivine	39.19		18.75		42.06						100.00
Apatite	0.15					54.25				41.06	95.46
Ti-magnetite	0.13	0.08	93.00	0.03	0.02	0.04			0.05		93.35
Biotite	33.00	15.00	30.00	0.80	3.50	0.07	0.06	9.40			91.83
Aegirine	51.79	1.68	27.82	0.51	1.75	5.10	10.85		0.13		99.63
Nepheline	42.60	34.20	0.38			0.15	15.91	6.50			99.74
Plagioclase	68.56	19.44	0.08				11.53	0.09			99.70

Note: data in wt.%; initial bulk melt = average Lofdal phono-tephrite composition; K-Feldspar, apatite, Ti-magnetite, biotite, aegirine, nepheline and plagioclase = average compositions

Fractionation assemblage	**K-fsp**	**Ol**	**Apa**	**Ti-mgn**	**Aeg**	**Bt**	**Neph**	**Plag**		**Total**
Proportions of fractionating minerals	96	0	0	0	0	0	4	0		100

Bodeving, S., Williams-Jones, A.E., Swinden, S., 2017. Carbonate–silicate melt immiscibility, REE mineralising fluids, and the evolution of the Lofdal Intrusive Suite, Namibia. Lithos 268–271, 383-398. http://dx.doi.org/10.1016/j.lithos.2016.11.024.

ESM_1

Click here to download Background dataset for online publication only: ESM_1.xlsx

Bodeving, S., Williams-Jones, A.E., Swinden, S., 2017. Carbonate–silicate melt immiscibility, REE mineralising fluids, and the evolution of the Lofdal Intrusive Suite, Namibia. Lithos 268–271, 383-398. http://dx.doi.org/10.1016/j.lithos.2016.11.024.

ESM_2

Click here to download Background dataset for online publication only: ESM_2.pdf

Bodeving, S., Williams-Jones, A.E., Swinden, S., 2017. Carbonate–silicate melt immiscibility, REE mineralising fluids, and the evolution of the Lofdal Intrusive Suite, Namibia. Lithos 268–271, 383-398. http://dx.doi.org/10.1016/j.lithos.2016.11.024.